



HAL
open science

Orbital forcing in southern Africa: towards a conceptual model for predicting deep time environmental change from an incomplete proxy record

Brian M. Chase

► To cite this version:

Brian M. Chase. Orbital forcing in southern Africa: towards a conceptual model for predicting deep time environmental change from an incomplete proxy record. *Quaternary Science Reviews*, 2021, 265, pp.107050. 10.1016/j.quascirev.2021.107050 . hal-03312268

HAL Id: hal-03312268

<https://hal.science/hal-03312268>

Submitted on 2 Aug 2021

HAL is a multi-disciplinary open access archive for the deposit and dissemination of scientific research documents, whether they are published or not. The documents may come from teaching and research institutions in France or abroad, or from public or private research centers.

L'archive ouverte pluridisciplinaire **HAL**, est destinée au dépôt et à la diffusion de documents scientifiques de niveau recherche, publiés ou non, émanant des établissements d'enseignement et de recherche français ou étrangers, des laboratoires publics ou privés.

1 Orbital forcing in southern Africa: towards a conceptual
2 model for predicting deep time environmental change from
3 an incomplete proxy record

4
5 **The author does not recommend the distribution of this**
6 **version of this article.**

7 **The article is freely available upon request.**

8 **To receive a copy, please send a request to Brian Chase at:**
9 **brian.chase@umontpellier.fr**

10
11
12 Brian M. Chase

13
14 *Institut des Sciences de l'Evolution-Montpellier (ISEM), University of Montpellier, Centre National de*
15 *la Recherche Scientifique (CNRS), EPHE, IRD, Montpellier, France;*

16
17 Correspondence and requests should be addressed to: Brian.Chase@umontpellier.fr,

18 +33 (0)6 01 06 64 04

20 Abstract

21 Southern Africa hosts regions of exceptional biodiversity and is rich with evidence for the presence and
22 activities of early humans. However, few records exist of the concurrent changes in climate that may
23 have shaped the region's ecological evolution and the development and dispersal of our ancestors.
24 This lack of evidence limits our ability to draw meaningful inferences between important changes in
25 the global and regional climate systems and their potential influence in shaping the region's natural
26 and cultural history. This paper synthesises the data currently available to define a general empirically-
27 based conceptual model of the spatio-temporal dynamics of climate change as they relate to changes
28 in the earth's orbital configurations. The goal is to identify mechanistic links between orbital forcing,
29 which can be calculated continuously over the past several million years, and environmental responses
30 to related changes in the major atmospheric and oceanic circulation systems influencing southern
31 Africa. Once identified, these relationships can be used to infer the most likely trends and patterns of
32 climate variability for periods and regions for which proxy evidence is not available.

33 Findings indicate that coherent patterns of change can be observed at wavelengths associated
34 with ~400-kyr and ~100-kyr cycles of orbital eccentricity. In southeastern Africa, the ~2400-kyr grand
35 cycle in eccentricity may have had an influence long-term patterns of aridification and humidification,
36 and the stronger ~400-kyr eccentricity cycle has a significant influence across inter-tropical Africa,
37 through changes in hydroclimate and monsoon circulation. The attribution of the ~100-kyr cycle to
38 specific orbital controls depends on location, as it can be determined by eccentricity-modulated direct
39 insolation forcing or through the combined orbital parameters and earth system responses that drive
40 the evolution of Pleistocene glacial-interglacial cycles.

41 Following the onset of the mid-Pleistocene transition (c. 1250-700 ka), the increasing
42 development of substantial polar ice sheets influence the nature of high-latitude drivers in southern
43 Africa. In southwestern Africa, records indicate an evolution in climate and circulation systems strongly
44 correlated with the global benthic $\delta^{18}\text{O}$ record, suggesting a particular sensitivity to high latitude
45 forcing. The close correlation between ~100-kyr eccentricity and glacial-interglacial cycles makes it
46 difficult to determine whether high- or low-latitude drivers dominate in southeastern Africa, but the
47 spatio-temporal patterning of environmental variability in many records are generally considered to
48 indicate a degree of high-latitude influence. Records from southeastern and southernmost Africa also
49 indicate that the influence of low latitude forcing, expressed through the local precessional cycle, is –
50 at least over the last glacial-interglacial cycles - dependent on eccentricity. Periods of reduced
51 eccentricity, particularly during periods of extensive high-latitude ice sheet development, result in
52 diminished influence in direct forcing and an increase in the expression of high latitude forcing, and an

53 increasingly positive correlation between the northern and southern tropics at these wavelengths. In
54 general, the records available allow for a simple conceptual model of the relationship between orbital
55 parameters and regional climates to be defined, with the strongest relationships existing at longer
56 timescales, such as the ~400-kyr eccentricity cycle. At finer spatio-temporal timescales, the data
57 indicate degrees of complexity that are not readily predicted, but the expansion of the regional dataset
58 will continue to allow for refinements to the conceptual model described.

59

60 Introduction

61 Knowledge of past environmental change in southern Africa is fundamentally limited by a lack of
62 evidence. This is largely due to southern Africa's arid to semi-arid environment, which hinders the
63 development of permanent lakes south of $\sim 15^{\circ}\text{S}$. Without such perennial, protected sediment traps,
64 terrestrial records are rare. Where records have been recovered, they are often discontinuous and
65 poorly dated (see Chase and Meadows, 2007). Only three terrestrial records from the region, from
66 Lake Malawi (Johnson et al., 2016), Tswaing Crater (Partridge et al., 1997) and Pinnacle Point (Braun
67 et al., 2019) encompass more than the last glacial-interglacial cycle (125 kyr). Broader inferences
68 relating to the influence of orbital forcing on regional climates may thus only be drawn from 1) proxy
69 data recovered from marine records, which may preserve longer sedimentary sequences of both
70 marine and terrestrial origin, and 2) by extrapolation of relationships observed between these data
71 and terrestrial records from more recent portions of the geological record. Further complicating this
72 research is the recognition that prevailing conceptual models for regional climate change only have
73 limited predictive capabilities, and that significant variability is the result of more complex processes
74 (e.g. Chase et al., 2017), resulting in substantially greater spatio-temporal heterogeneity in signals of
75 environmental change (Chase et al., in press; Chase et al., 2019a; Chase and Quick, 2018; Chevalier and
76 Chase, 2015).

77 This paper reviews: 1) the general framework of the southern African climate systems that are
78 considered to have driven the major trends in environmental variability during the late Quaternary,
79 and 2) how mechanisms both external (i.e. orbital parameters) and internal (e.g. continental ice sheets,
80 CO_2) to the earth system may influence these systems. The goal is to provide a general model for the
81 use of orbital parameters to infer past climate conditions and trends for periods from which proxy data
82 is not available.

83 Southern African climate systems

84 Southern Africa (considered to be 0° - 35°S for the purpose of this paper) experiences much greater
85 climatic diversity than its Northern Hemisphere counterpart (Peel et al., 2007). This is due to a series
86 of factors related to the continent's morphology and latitudinal position. While northern Africa is, with
87 the addition of the Arabian Peninsula, nearly 8,000 km across from east to west, southern Africa is just
88 over 3,000 km across. This relatively small area limits the development of high pressure over the
89 continent and enables the effective incursion of moist air from the adjacent tropical Indian and Atlantic
90 oceans. In the east, the warmth of the Agulhas Current fosters increased evaporation and the transport
91 of moisture into the interior (Crétat et al., 2012; Rouault et al., 2002; Tyson and Preston-Whyte, 2000).
92 In the west, tropical moisture advection from the Atlantic Ocean is generally limited to regions north

93 of ~15°S (Crétat et al., 2019; Rouault et al., 2003). Further south, the cold Benguela Current flows
94 equatorward along the South African and Namibian coasts, limiting evaporation and suppressing
95 convection (Nicholson and Entekhabi, 1987; Tyson, 1986). As a result, a marked east-west rainfall
96 gradient exists across the subcontinent at these latitudes, and the dominant moisture-bearing systems
97 are northerly flow over Angola and easterly flow from the Indian Ocean. Southern African climates are
98 also strongly influenced by extra-tropical systems. Poleward of the subcontinent, the southern
99 westerlies dominate mid-latitude atmospheric circulation. Perturbations in the westerlies create fronts
100 that produce the majority of rainfall received by the southwestern Cape (Reason et al., 2002). The
101 influences of these various systems have strong seasonal biases, with the tropical systems being most
102 vigorous in the warm summer months, and the extra-tropical frontal systems being most prevalent
103 during the winter, when the Antarctic anticyclone expands and the zone of frontal activity is displaced
104 equatorward (Figure 1).

105 The diversity and distribution of atmospheric and oceanic circulation systems influencing
106 southern Africa has led to regional distinctions based on the seasonal distribution of rainfall, with most
107 of the subcontinent comprising the summer rainfall zone (SRZ), and the extreme southwestern margin
108 being referred to as the winter rainfall zone (WRZ) (Figure 1). Between the SRZ and the WRZ is a
109 transitional zone, which is influenced by both tropical and temperate systems. This has been referred
110 to variously as the year-round rainfall zone (YRZ), all-year rainfall zone or aseasonal rainfall zone (ARZ).
111 The criteria by which these regions have been defined varies, but a commonly employed method is
112 the percentage of mean annual rainfall during the winter (>66% = WRZ, <33% = SRZ, 33%-
113 66%=YRZ/ARZ; sensu Chase and Meadows, 2007)(Figure 1). Climates in each of these broad regions
114 are highly variable, ranging significantly in terms of the amount of mean annual precipitation received,
115 but the purpose of their definition is to delimit the spatial influence of southern Africa's dominant
116 moisture-bearing systems and thereby develop mechanistic models for their past variability.

117 [Orbital mechanisms driving long-term climate variability in southern Africa](#)

118 At their broadest scale, Quaternary climate dynamics are understood to be paced by changes in the
119 Earth's orbital parameters (Berger et al., 1984; Chappell, 1973; Hays et al., 1976; Imbrie, 1982; Imbrie
120 et al., 1984; Milankovitch, 1930). These changes include the shape of the Earth's orbit (eccentricity),
121 the degree of Earth's axial tilt (obliquity) and the direction of the axis at a defined point of Earth's
122 motion around the sun (precession). Each of these parameters varies at quasi-regular cycles:
123 eccentricity expressing ~400,000-year and ~100,000-year cycles, obliquity expressing a ~41,000-year
124 cycle, and precession expressing a ~23,000-year cycle. Respectively, these variables influence the
125 amount of solar insolation the Earth receives, the intensity of the seasons, and the season in which the
126 Earth is closest to the sun and receiving the most insolation. While it is generally accepted that these

127 orbital changes have paced the timing and amplitude of the glacial and interglacial periods of the
128 Quaternary, their influence on long-term southern African climate change has been a matter of debate
129 (e.g. Chase et al., 2019b; Collins et al., 2014; Dupont et al., 2011; Partridge et al., 1997; Stuut et al.,
130 2002).

131 The discussion of the role of orbital forcing on southern African climates has often been
132 structured in terms of remote (high latitude) versus direct (low latitude) mechanisms (Partridge et al.,
133 1997; Thomas and Shaw, 2002; van Zinderen Bakker, 1976). High latitude mechanisms relate to the
134 development of high latitude ice sheets and the impact of their expansion and contraction (including
135 ice-rafting and meltwater pulses) on global atmospheric and oceanic circulation dynamics (Chase et
136 al., 2015; Chevalier and Chase, 2015; Otto-Bliesner et al., 2014; Schefuß et al., 2011; Stuut and Lamy,
137 2004; Stuut et al., 2002; van Zinderen Bakker, 1967). Consideration of low latitude forcing generally
138 relates to precession-driven changes in insolation seasonality, and their quasi-direct impact on regional
139 and local precipitation through their influence on the development of convective and monsoonal
140 systems (Kutzbach, 1981; Kutzbach et al., 2020; Partridge et al., 1997; Rossignol-Strick, 1983;
141 Ruddiman, 2006b; Street-Perrott et al., 1990).

142 In southern Africa, high latitude forcing underpins the broadest conceptual models (Cockcroft
143 et al., 1987; van Zinderen Bakker, 1976) and is also considered to be a significant factor in driving some
144 abrupt climate change events (e.g. those associated with Heinrich stadial 1 and the Younger Dryas)
145 (Chase et al., 2015; Chase et al., 2011; Schefuß et al., 2011). Broadly, these changes are related to
146 global temperature variability, Northern Hemisphere ice-sheet development and dynamics, and
147 Antarctic sea-ice extent. Global cooling – initiated by declining high latitude Northern Hemisphere
148 summer insolation (Milankovitch, 1930), eccentricity (Broecker and van Donk, 1970; Hays et al., 1976)
149 and the development of major ice-sheets (Ruddiman, 2006a) – is considered to have resulted in a
150 decrease in rainfall in the SRZ through a reduction in evaporative and convective potential, and thus a
151 reduction in the amount of moisture advection from adjacent oceans and the potential for
152 precipitation events (Cockcroft et al., 1987; van Zinderen Bakker, 1976). In the WRZ, it is thought that
153 this same cooling would have resulted in an expansion of Antarctic sea-ice, an expansion of the circum-
154 polar vortex, and an equatorward shift of the storm tracks embedded in the southern westerlies,
155 resulting in an increased occurrence of precipitation events in southwestern Africa (Cockcroft et al.,
156 1987; Stuut et al., 2004; van Zinderen Bakker, 1976).

157 Considering southern Africa's largely tropical-subtropical position, it is not surprising that an
158 abundance of evidence exists indicating a strong influence of direct insolation forcing on regional
159 climates. This evidence has been obtained from both terrestrial (Chase et al., 2019b; Partridge et al.,

160 1997) and marine sediment records (Collins et al., 2014; Simon et al., 2015), and discussions primarily
161 relate to variability in orbital precession (~23-kyr cycle) and changes in the range of the African tropical
162 rainbelt (sometimes considered to be synonymous with the intertropical convergence zone (ITCZ))
163 tracking the zone of maximum summer insolation. While notable exceptions exist (e.g. southwestern
164 Africa; Chase et al., 2019b), changes in hydroclimate associated with precessional forcing generally
165 manifest as more (less) summer rainfall under higher (lower) summer insolation. Related to seasonal
166 precipitation and insolation, these changes are thought to have been anti-phase between the Northern
167 and Southern hemispheres (Kutzbach, 1981; Ruddiman, 2006b), but their strength in both
168 hemispheres is directly related to changes in eccentricity, which determines the amount of insolation
169 received. At high latitudes, eccentricity plays a role in determining the timing and duration of glacial
170 cycles, particularly after mid-Pleistocene transition (MPT; ~1250 - 700 ka; Clark et al., 2006; Lisiecki
171 and Raymo, 2005; Mudelsee and Schulz, 1997). It should be noted that this role is neither dominant
172 nor isolated, as is sometimes assumed based on the similarity between the ~100-kyr eccentricity cycle
173 and the average length of late Pleistocene glacial periods. Rather, eccentricity's influence is effected
174 through its impact on precession, which works in concert with obliquity to establish the timing of
175 glacial-interglacial cycles (Bajo et al., 2020; Huybers, 2006, 2011; Tzedakis et al., 2017). At low latitudes,
176 eccentricity and precession have a more direct influence on climate, and, as will be shown, can be used
177 as strong predictors of low latitude climate change over even longer timescales, extending back
178 millions of years.

179 Eccentricity

180 *2400-kyr grand eccentricity cycle*

181 While precession is perhaps the most commonly considered parameter in southern Africa – as its
182 strength and frequency make it most relevant to studies of late Quaternary low latitude climate change
183 – changes in the precessional index are modulated by changes in eccentricity. Eccentricity varies at
184 two primary periods relevant to Quaternary science, ~400-kyr and ~100-kyr, but longer “grand cycles”
185 also exist, such as the 2400-kyr cycle (Boulila et al., 2012; Laskar et al., 2004; Olsen and Kent, 1996;
186 Pälike et al., 2006a). While much weaker (Figure 2), these cycles have been highlighted as being
187 significant environmental determinants over long, $>10^6$ yr⁻¹ timescales (Crampton et al., 2018; Pälike
188 et al., 2006b). During the Quaternary Period, these cycles may also have had some influence, as there
189 is a degree of consistency with long-term trends of Pleistocene hydroclimate in southeastern Africa.
190 Records of terrestrial sediment flux in marine cores MD96-2048 (Caley et al., 2018) and IODP Site
191 U1478 (Koutsodendris et al., 2021) off the Limpopo River mouth has been interpreted as reflecting
192 regional rainfall variability, and from Lake Malawi a $\delta^{13}\text{C}$ record obtained from leaf waxes is interpreted
193 as an indicator of vegetation and associated environmental change (Johnson et al., 2016). It should be

194 noted that while complexities regarding the interpretation of the $\delta^{13}\text{C}_{\text{wax}}$ have been highlighted (Ivory
195 et al., 2018), its coherent relationship with other hydroclimatic proxies from Lake Malawi (e.g. lake
196 level; Lyons et al., 2015) is considered here to render it suitable for inclusion. At the scale of the 2400-
197 kyr grand cycle in eccentricity, the MD96-2048 and U1478 records indicate patterns of variability prior
198 to ~500-600 ka that would be consistent with a positive relationship between eccentricity and rainfall
199 (Figure 3). At Lake Malawi, a similarly consistent, but opposite trend is observed, with increasingly
200 humid conditions being inferred across the last million years (Johnson et al., 2016; Lyons et al., 2015).
201 This spatio-temporal patterning of trends has been considered to indicate an equatorward shift of the
202 southern limit of the African rainbelt (Caley et al., 2018), which is consistent with reconstructions of
203 dynamics from more recent portions of the geological record (Chevalier and Chase, 2015). That this
204 signal is not apparent in the LR04 global benthic foraminifera $\delta^{18}\text{O}$ record (Lisiecki and Raymo, 2005),
205 which reflects changes in global ice volume, suggests that its influence may be restricted to lower
206 latitudes. The marked deviation from the positive relationship between the 2400-kyr eccentricity cycle
207 and terrestrial sediment flux in the Limpopo marine cores, particularly U1478, may relate to
208 fundamental changes in global circulation systems after the MPT as a result of more extensive high
209 latitude ice sheets and lower CO_2 . It should be noted, however, that the chronology of the U1478
210 record is currently not based on based on an independent oxygen isotope stratigraphy, but employs
211 the $\ln(\text{Ti}/\text{Ca})$ record in an interpretive paradigm that presupposes a negative relationship between
212 eccentricity and rainfall (Koutsodendris et al., 2021). The result differs notably from the chronology of
213 the adjacent M96-2048, complicating consideration and comparison at this stage.

214 *~400-kyr eccentricity cycle*

215 Considering that the ~400-kyr cycle is the strongest and most consistent of the eccentricity cycles
216 (Figure 2), the expectation is that it will have been a significant determinant of long-term low latitude
217 climate change, with increased tropical rainfall during periods of higher eccentricity. Across Africa, the
218 response and interpretations of several long proxy records highlight different aspects of the
219 environmental change related to eccentricity (Figure 4). The ODP 967 “wet/dry index” (Grant et al.,
220 2017), for example, has been interpreted as having a strong relationship with hydroclimatic variability
221 and exhibits a positive relationship with the ~400-kyr eccentricity cycle. In contrast, the dust flux
222 records from ODP 659 (off West Africa; Tiedemann et al., 1994) and ODP 721/722 (off southeastern
223 Arabia; deMenocal, 1995) have been interpreted in a way that indicates a negative relationship
224 between humidity and the ~400-kyr eccentricity cycle (higher dust flux during periods of high
225 eccentricity). The relationship between dust flux and climate is, however, likely more complex (cf.
226 Trauth et al., 2009). One mechanism controlling variability in these records is almost certainly aridity,
227 and the related erodibility of the landscape, as the original authors indicate. This aspect of

228 environmental change likely explains the overall increase in dust flux to these sites across the
229 Pleistocene, with the expansion of Northern Hemisphere ice sheets, the establishment of strong
230 Walker circulation (Ravelo et al., 2004), and more significant arid periods in the Sahara. The positive
231 correlation between eccentricity and records of both aridity (ODP 659 and ODP 721/722) and humidity
232 (ODP 967, MD96-2048) at ~400-kyr frequencies, however, demands further consideration, particularly
233 as sites such as Lake Magadi in Kenya (Owen et al., 2018) and Mukalla Cave (Nicholson et al., 2020),
234 adjacent to ODP 721/722, indicate more humid conditions under high eccentricity at this frequency.
235 Trauth et al. (2009) have suggested that dust fluxes at ODP 659 and ODP 721/722 may be significantly
236 influenced by changes in monsoon circulation, with periods of high eccentricity resulting in increased
237 aeolian sediment transport to the sites. It seems likely that the dust records are influenced by both
238 direct insolation, particularly the ~400-kyr eccentricity cycle, and high-latitude forcing, which becomes
239 a dominant control with the development of the ~100-kyr cycle after the onset of the MPT.

240 As with the 2400-kyr cycle, there are few records available from southern Africa that are long
241 enough to be used to confirm and explore the influence of the ~400-kyr cycle. Again, MD96-2048 and
242 Lake Malawi (Johnson et al., 2016; Lyons et al., 2015) have provided the best continuous records to
243 date, and both express a ~400-kyr cycle of hydroclimatic variability (Figure 4). Similar to responses
244 associated with the 2400-kyr cycle, the Lake Malawi lake level record (Lyons et al., 2015) exhibits a
245 negative relationship with the ~400-kyr eccentricity cycle, while the MD96-2048 Fe/Ca terrestrial
246 discharge record (Caley et al., 2018) correlates positively with eccentricity at this frequency, as does
247 the lower resolution record of flowstone development from South Africa's Cradle of Humankind
248 (Pickering et al., 2019) (Figure 4). It is interesting to note that while the strength of the ~400-kyr signal
249 in the Lake Malawi record increases over the last 1300 kyr, it diminishes in the MD96-2048 Fe/Ca
250 record. This also broadly coincides with the MPT and the change in dominance from ~41-kyr to ~100-
251 kyr cycles in the LR04 global benthic foraminifera $\delta^{18}\text{O}$ record (Lisiecki and Raymo, 2005) and significant
252 Northern Hemisphere ice sheet expansion. As with the circulation dynamics relating to the
253 establishment of wetter conditions in the Zambezi region while regions to the north and south become
254 more arid seems linked to Northern Hemisphere cooling (Chevalier and Chase, 2015; Schefuß et al.,
255 2011; Wang et al., 2013), it may be that this trend is associated with the post-MPT development of
256 high latitude ice sheets and perhaps the related development of a more strongly positive Indian Ocean
257 Dipole (Johnson et al., 2016; Taylor et al., in press; Wang et al., 2015). The concurrent decrease in the
258 ~400-kyr signal in the MD96-2048 Fe/Ca record may be a corollary of this same reorganisation of
259 atmospheric and oceanic circulation systems influencing the region, also reflecting a shift from low-
260 latitude forcing dominance in southern Africa to a scenario in which high-latitude forcing plays a more
261 significant role.

262 In southwestern Africa, sea-surface temperature records (SSTs) from the ODP175-1082
263 (Etourneau et al., 2009) and ODP175-1084 marine cores (Marlow et al., 2000) from the Benguela
264 Upwelling System (Figure 1) spanning the last 4600-kyr do not exhibit a strong ~400-kyr cyclicity
265 consistent with eccentricity. This is similar to the response of the LR04 $\delta^{18}\text{O}$ record (Lisiecki and Raymo,
266 2005), which also exhibits extremely limited variability at this frequency (although the LR04 curve does
267 express a generally negative relationship with eccentricity at this frequency prior to the MPT). The ODP
268 1082 and 1084 records, however, do show strong similarities with the LR04 record, both in its overall
269 Plio-Pleistocene pattern (decreasing SSTs with increase global ice volume), and the development of an
270 increasingly clear ~100-kyr cycle following the MPT (Figure 6).

271 *~100-kyr cycles*

272 Following the MPT, c. 1250-700 ka, a ~100-kyr glacial-interglacial cycle became a much more significant
273 aspect of global climate change (Clark et al., 2006; Lisiecki and Raymo, 2005; Mudelsee and Schulz,
274 1997). The drivers of this cycle remain a topic of active inquiry (e.g. Bajo et al., 2020), as the inception
275 of prominent interglacial periods are not thought to be determined by the ~100-kyr eccentricity cycle
276 per se - as may be inferred - but by the combined influence of precession and obliquity, with glacial
277 periods of the late Pleistocene typically lasting two or three obliquity cycles (80 and 120 years, resulting
278 in an average ~100-kyr periodicity) (Huybers, 2006, 2011; Tzedakis et al., 2017). This does not,
279 however, mean the ~100-kyr eccentricity cycle has no influence, as it modulates the precessional cycle
280 and is thus a significant factor in determining when insolation thresholds are crossed. In southern
281 Africa, the source of the ~100-kyr cyclicities observed in fossil records depends on whether high or low
282 latitude drivers are the dominant controls of regional climate dynamics. In regions dominated by high
283 latitude drivers, changes observed at this wavelength are most likely attributable to the influence of
284 obliquity and precession at high northern latitudes and the development of associated ice sheets. In
285 tropical regions, particularly during periods of Earth's history when significant high latitude ice sheets
286 were not present, variability at ~100-kyr cyclicities may more likely be driven by changes in direct
287 insolation as modulated by eccentricity.

288 The importance of ~100-kyr cycles is evident in only some of the southeastern African records
289 that extend back over multiple cycles. For example, the MD96-2048 Fe/Ca (Caley et al., 2018) and leaf
290 wax $\delta^{13}\text{C}$ records (Castañeda et al., 2016) suggest phases of increased humidity that correlate well with
291 higher eccentricity. Other records, such as those from Lake Malawi are more ambiguous, with a ~100-
292 kyr cycle being only weakly expressed (Johnson et al., 2016; Lyons et al., 2015), and the Fe/K record
293 from marine core CD154-10-06P (Simon et al., 2015) indicates – if anything – an opposing response.
294 These differences may relate to changes in spatial climate response gradients during the Pleistocene,
295 complex responses to the influences of high and low latitude forcing mechanisms, or limitations

296 imposed by the chronologies of some sites. Establishing coherent scenarios that adequately explain
297 the spatio-temporal variability observed across the region remains an area of active research.

298 As mentioned above, southeast Atlantic SSTs (Etourneau et al., 2009; Marlow et al., 2000)
299 exhibit a strong positive correlation with the LR04 benthic $\delta^{18}\text{O}$ record (Lisiecki and Raymo, 2005),
300 including ~ 100 -kyr cycles, indicating a strong high latitude influence. Dust records from adjacent
301 marine cores MD96-2094 (Stuut et al., 2002) and MD96-2087 (Pichevin et al., 2005) indicate more
302 aeolian sediment transport under stronger wind fields during glacial periods; linked with SSTs through
303 upwelling and intensifications of the South Atlantic Anticyclone (Etourneau et al., 2009; Little et al.,
304 1997; Marlow et al., 2000). The dust records have been employed to infer environmental conditions
305 in southwestern Africa, with greater proportions of fine sediments being interpreted as indicating
306 increased fluvial activity and increased humidity (Stuut et al., 2002). This interpretation demonstrates
307 – as with the SST records – a strong correlation with the LR04 record, suggesting that cooler global
308 conditions and more extensive polar ice sheets result in more humid conditions in the region. At these
309 timescales, and comparing glacial versus interglacial conditions, terrestrial records from the region
310 (Chase et al., 2019b; Lim et al., 2016; Scott et al., 2004), support these inferences, indicating that the
311 last glacial period was generally more humid than the Holocene, with changes in potential
312 evapotranspiration playing a significant role in determining regional water balance (with cooler periods
313 being generally more humid; Chase et al., 2019b; Lim et al., 2016). However, the available data do
314 highlight significant contradictions between marine and terrestrial records (a topic that will be
315 discussed in greater detail in the section addressing ~ 23 -kyr cycles) and care should be taken in
316 applying these findings to shorter timescales.

317 In terms of accurately attributing the source of a ~ 100 -kyr signal to low or high latitude
318 mechanisms, the presence of a ~ 400 -kyr signal and/or the dominance of a ~ 23 -kyr signal that is
319 consistent with direct insolation (e.g. the Botuverá Cave speleothem record from Brazil (Cruz Jr. et al.,
320 2005)), may provide indications of low latitude forcing dominance. Where these signals are absent or
321 strongly muted, and a significant ~ 41 -kyr signal is observed, high latitude mechanisms may more likely
322 be the source of the ~ 100 -kyr cycle.

323 *~ 41 -kyr obliquity cycle*

324 Obliquity (axial tilt) modulates the intensity of seasonality, and primarily affects higher latitudes. As
325 such – coupled with the length of the cycles in relation to the majority of available records – it is not
326 surprising that it has not often been identified as a prominent signal in southern African records. In
327 those records where a ~ 41 -kyr cycle can be identified, its origin has been associated with changes in
328 high northern latitude insolation and the related evolution of continental ice sheets. It may be

329 important to note, however, that in idealised modelling experiments it has been found that obliquity-
330 induced changes can be observed at low latitudes without changes in high latitude ice sheets (Bosmans
331 et al., 2015). Under high obliquity scenarios, increased cross-equatorial insolation and temperature
332 gradients draw increased moisture into the summer hemisphere, resulting in increased tropical
333 precipitation both north and south of the equator. The influence of this low latitude response remains
334 to be fully resolved, but it may have played a role in driving low latitude climate variability, particularly
335 during periods of low global ice volume.

336 In southwestern Africa, the ~41-kyr cycles that characterise changes in Plio-Pleistocene global
337 ice volume prior to the MPT (Lisiecki and Raymo, 2005) were apparently more significant prior to ~2000
338 ka in SE Atlantic SST records (Etourneau et al., 2009). In southeastern Africa, interpretations of
339 different records vary, perhaps at least in part as a function of their resolution. Caley et al. have
340 determined that SST and sea-surface salinity records from marine core MD96-2048 exhibit significant
341 ~41-kyr cycles (Caley et al., 2018; Caley et al., 2011), while records of changes in terrestrial
342 environments from the same core (Fe/Ca; Caley et al., 2018) are rather dominated by ~100-kyr and
343 ~23-kyr cycles, suggesting perhaps that precipitation in the region is linked to land-sea temperature
344 contrasts, rather than directly to SSTs (Caley et al., 2018). In contrast, the Plio-Pleistocene records from
345 the adjacent marine core ODP U1478 (Figure 1) reflecting changes in the same catchment contains
346 significant ~41-kyr cycles in both SSTs and leaf wax δD , suggesting that SSTs did have a direct influence
347 on terrestrial climates, at least during the 4000-1800 ka interval (Taylor et al., in press).

348 Over the last ~200 kyr, the bulk $\delta^{13}C$ record from Lake Malawi (Lyons et al., 2015) contains a
349 significant ~41-kyr cycle as part of a pattern of variability that bears marked similarities to the glacial-
350 interglacial periods registered in the LR04 benthic $\delta^{18}O$ record (Lisiecki and Raymo, 2005).
351 Palaeovegetation records from marine core MD96-2048 (Castañeda et al., 2016; Dupont et al., 2011)
352 also reveal changes similar to the glacial-interglacial cycles reflected in the LR04 record, but these
353 patterns contrast with the MD96-2048 Fe/Ca record (Caley et al., 2018), perhaps indicating that
354 vegetation change in the basin was more significantly influenced by temperature (Chevalier et al.,
355 2020) or CO_2 (Dupont et al., 2019). At these shorter timescales, however, the MD96-2048 Fe/Ca record
356 is also at odds with other regional records that have similarly been interpreted as reflecting changes
357 in regional hydroclimates (Chevalier and Chase, 2015; Holmgren et al., 2003; Partridge et al., 1997),
358 suggesting complexities in either the spatio-temporal patterning of climate anomalies or in the
359 interpretation of the various proxies.

360 To further explore the nature of the response to changes in obliquity in SE Africa, semblance
361 analysis (Cooper and Cowan, 2008) was used to analyse the relationship between terrestrial sediment

362 flux from the Limpopo River (interpreted as a proxy for rainfall) and global ice volume. Employing,
363 respectively, the MD96-2048 $\ln(\text{Fe}/\text{Ca})$ record (Caley et al., 2018) and the LR04 benthic $\delta^{18}\text{O}$ record
364 (Lisiecki and Raymo, 2005), and isolating the 41-kyr obliquity frequency, it can be observed that the
365 correlation between terrestrial sediment flux and global ice volume associated with axial tilt has
366 alternated between positive (more rainfall during glacial periods) and negative (less rainfall during
367 glacial periods) states (Figure 7). Interestingly, considering the 400-kyr component of these results, a
368 pattern of variability consistent with the expansion of continental ice sheets across the last 2140 kyr is
369 apparent. Prior to the MPT, increased ice volume is generally negatively correlated with runoff from
370 the Limpopo Basin. During this period, long-term shifts toward a more positive relationship between
371 runoff and ice volume occur during phases of increased eccentricity, suggesting a dynamic of wetter
372 conditions during higher obliquity with eccentricity acting as a significant modulator. This may indicate
373 1) a muting of tropical rainfall even during the weak pre-MPT glacial periods, and/or 2) a scenario in
374 which increased obliquity affects regional climates through an increase in cross-equatorial
375 temperature gradients and strengthened summer moisture transport (Bosmans et al., 2015), a
376 dynamic that may be amplified under higher eccentricity and insolation. The MPT marks an important
377 threshold in the relationship between orbital parameters, ice volume and SE African climate. During
378 and after the MPT, the correlation between Limpopo River runoff and obliquity-induced changes in ice
379 volume becomes more often positive, indicating increased runoff during phases of low obliquity.
380 Significantly, this dynamic is most prevalent during periods of low eccentricity, when low latitude
381 forcing is weakened, supporting the proposal that the relative strength of high and low latitude forcing
382 mechanisms is critical for ascertaining the regional response to changes in orbital parameters (Chase
383 et al., in press).

384

385 *~23-kyr precessional cycles*

386 The ~23-kyr cycle of orbital precession is, by virtue of its relatively short length as well as southern
387 Africa's generally low latitude position, the most widely recognised orbital cycle observed in the
388 regional records available (e.g. Collins et al., 2014; Partridge et al., 1997; Simon et al., 2015). Its nature
389 as a determinant of the seasonal distribution of solar insolation means that the cycle engenders an
390 antiphase response between the Northern and Southern hemispheres, with phases of high boreal
391 summer insolation also being phases of low austral summer insolation. As such, it has in some cases
392 led to contradictory interpretations of whether high or low latitude forcing is responsible for a given
393 ~23-kyr signal (cf. Collins et al., 2014; Stuut et al., 2002). In southwestern Africa, this can be
394 conceptualised either as an expansion/intensification of tropical systems and increased summer
395 rainfall under increased direct summer insolation (e.g. Collins et al., 2014), or, alternatively, as an

396 expansion/shift of the southern westerlies and increase in winter rainfall during cooler conditions
397 induced by reduced high latitude boreal summer insolation (e.g. Stuu et al., 2002). In southeastern
398 Africa, this dichotomy can be considered in terms of push and pull factors, with the African tropical
399 rainbelt either being displaced southward as a result of Northern Hemisphere cooling (e.g. Schefuß et
400 al., 2011), or drawn southward as it tracks the zone of maximum summer insolation (e.g. Partridge et
401 al., 1997).

402 In southern Africa, the influence of precessional forcing appears to be both temporally and
403 spatially variable. In southeastern Africa, evidence from lacustrine sediments from Tswaing Crater
404 (Partridge et al., 1997) and from the marine core CD154 10-06P Fe/K record (Simon et al., 2015) (Figure
405 1) both indicate a strong precessional signal. It should be noted that the Tswaing Crater record of
406 Partridge et al. (1997) was, based on its dominant 23-kyr cycle, tuned slightly to precession to improve
407 its chronology for the period between the oldest radiocarbon age and the basal fission track age
408 estimate. While initially contentious, this tuning is now supported by records such as the CD154 10-
409 06P Fe/K record (Simon et al., 2015) and speleothem records from southernmost Africa's Cape Fold
410 Mountains (Braun et al., 2020; Chase et al., in press; Talma and Vogel, 1992). After approximately ~70
411 ka the relationship between precession and regional hydroclimates begins to break down (Figures 8
412 and 9), a dynamic that has been assessed and clarified by Chase et al. (in press) through comparisons
413 with the RC09-166 leaf wax δD record from the northern tropics in the Gulf of Aden (Tierney et al.,
414 2017) and Chinese speleothem composite $\delta^{18}O$ record (Cheng et al., 2016). Findings indicate that under
415 high eccentricity during MIS 5 southeast African tropical rainfall increased during periods of high local
416 insolation, antiphase to trends in the northern tropics and consistent with Kutzbach's orbital monsoon
417 hypothesis (Kutzbach, 1981). However, at ~70 ka – broadly concurrent with the establishment of pan-
418 Arctic ice sheets in MIS 4 (Batchelor et al., 2019) – rainfall variability in southeastern Africa adopts a
419 signal that is in-phase with the northern tropics. This in-phase relationship persists until the onset of
420 the Holocene, when high latitude ice sheets retreated and direct local insolation forcing once again
421 became the dominant driver of southeast African rainfall variability (Chase et al., in press). Additionally,
422 interpretation of the Cape Fold speleothem $\delta^{18}O$ record pre-dating the transition at ~70 ka is generally
423 consistent with changes in rainfall amount associated with the "amount effect" (Dansgaard, 1964;
424 Herrmann et al., 2017), consistent with an expanded summer rainfall zone. After ~70 ka, when an
425 obliquity cycle becomes apparent, speleothem $\delta^{18}O$ likely reflects changes in regional temperatures,
426 suggesting a change in rainfall regimes and a restriction of the zone of tropical dominance (Chase et
427 al., in press).

428 Along the southeast African margin, displacements of the African rainbelt associated with high
429 northern latitude forcing have been cited as a potential control on the spatio-temporal patterns of

430 orbital and sub-orbital climate variability across the last 50 kyr (Chevalier and Chase, 2015). Records
431 from eastern African lake sites such as Lake Tanganyika show clear affinities with high latitude
432 Northern Hemisphere signals, particularly during MIS 2 and the end of MIS 3 (~10-30 ka), when cold
433 conditions in the north, and particularly the North Atlantic basin, induce dry conditions at the site
434 (Tierney et al., 2008). As with the regionally anti-phase response of the Lake Malawi basin at longer
435 orbital timescales noted above, leaf wax δD records from marine cores GIK 16160-3 (Wang et al., 2013)
436 and GeoB 9307-3 (Schefuß et al., 2011) reflecting changes in the Zambezi Basin indicate an opposing
437 response, with the Last Glacial Maximum (LGM; 19-26.5 ka), Heinrich Stadial 1 (HS1; ~18-14.6 ka) and
438 the Younger Dryas (12.9-11.7 ka) experiencing increased rainfall, as the African rainbelt was displaced
439 to the south. To the south of the Zambezi, in South Africa, records indicate conditions similar to those
440 at Lake Tanganyika, apparently constraining the zone of increased precipitation during periods of
441 Northern Hemisphere cooling to a narrow band between ~15 and 20°S (Chevalier and Chase, 2015). As
442 the high latitude ice sheets diminished, CO₂ increased and global temperatures warmed, direct
443 precessional forcing once again became the dominant control on long-term climate change throughout
444 eastern Africa (Chevalier and Chase, 2015).

445 These findings have important implications for the use of Earth system/general circulation
446 models (ESMs/GCMs) to study past climate change dynamics in southern Africa. In these models,
447 insolation is a dominant determinant of low latitude climate change, and as such simulations of palaeo-
448 precipitation often exhibit patterns of variability consistent with precessional cycles (Gordon et al.,
449 2000; Pope et al., 2000), including relatively wetter conditions across much of southern Africa during
450 the LGM (Engelbrecht et al., 2019; Schmidt et al., 2014; Sueyoshi et al., 2013). Regional data-model
451 comparisons, however, indicate that when direct insolation forcing is reduced during phases of low
452 eccentricity other drivers may become more significant (Singarayer and Burrough, 2015), that ESM
453 performance may be limited in the region (Chevalier et al., 2017) and that such simulations should only
454 be employed with due caution.

455 It should be considered too in terms of low latitude forcing that phases of high eccentricity and
456 strong precessional influence may experience much wetter conditions during summer insolation
457 maxima, but they also appear – at least in some cases – to experience much drier periods during
458 summer insolation minima, and long-term climatic variability tends to increase (Lyons et al., 2015;
459 Scholz et al., 2007). Despite this increased variability, the MD96-2048 record (Caley et al., 2018),
460 indicates increases in mean humidity consistent with ~2400-kyr, ~400-kyr and ~100-kyr eccentricity
461 cycles, suggesting that at least in the Limpopo catchment, phases of high eccentricity are associated
462 with higher humidity.

463 Considering the spatial variability of precessional signals, data from a series of rock hyrax
464 middens from the Namib Desert region on the western margin of southern Africa provide evidence of
465 the influence of precession over the last 50 kyr. In this region, periods of high summer insolation are
466 characterised by increased aridity (Chase et al., 2019b). This reflects the combined influence of higher
467 low latitude insolation reducing atmospheric pressure over the continent, with concomitant high
468 latitude cooling and steeper hemispheric temperature gradients resulting in intensifications of the
469 South Atlantic Anticyclone. The increased land-sea pressure gradient led to the advection of cold air
470 off the SE Atlantic, and drier conditions in the Namib Desert. These findings do raise questions about
471 the inferences made regarding marine records recovered offshore from Namibia, such as the MD08-
472 3167 leaf wax δD record, which indicates a positive relationship between precipitation and summer
473 insolation (Collins et al., 2014). One possibility indicated by the authors is that the source of the
474 sediment fractions analysed for this record lies to the north or east of the Namib Desert. The
475 persistence of the precessional signal from 10-70 ka (Figure 10) suggests that the source area is not as
476 far east as Tswaing Crater. However, the Makgadikgadi basin of the middle Kalahari is a major dust
477 source (Vickery et al., 2013), and the MD08-3167 data may thus reflect conditions in this region. This
478 spatial heterogeneity of signals may also relate to past dynamics of the Congo Air Boundary, which is
479 defined by the boundary between Atlantic and Indian ocean air masses, and is associated with the
480 southern margin of the African rainbelt in southwestern Africa (Howard and Washington, 2019), and
481 has been invoked as a possible explanation for some aspects of palaeoclimatic variability in the
482 Makgadikgadi region (Cordova et al., 2017). It should be noted, however, that the few records available
483 from this region appear to indicate relatively humid Holocene conditions (Burrough et al., 2009;
484 Burrough et al., 2007; Cordova et al., 2017). While consistent with a precessional driver, these findings
485 contrast with the MD08-3167 data, which exhibits a markedly drier Holocene (Collins et al., 2014).

486 Another possibility is that rather than relating to changes in terrestrial environments, the
487 marine core records of the southeast Atlantic are strongly influenced by changes in terrigenous
488 sediment source region related to the strength and position of the southeast trade winds and the
489 descending limb of the South Atlantic Anticyclone (Figure 11). This is suggested by the periodic
490 inclusion of significant percentages of Restionaceae pollen (Cape reeds) in the region's marine
491 sediments (Shi et al., 2001), despite no concurrent changes in this taxon being found at terrestrial sites
492 from the Namib or Kalahari regions (Cordova et al., 2017; Lim et al., 2016; Scott et al., 2004). Variability
493 of this wind field maintains a strong precessional signal throughout the last glacial period, driven as it
494 is in part by changes in inter- and intra-hemispheric temperature gradients that are most pronounced
495 during glacial periods and most particularly phases of pronounced high-latitude cooling associated
496 with decreased boreal summer insolation (Figure 11). As such, it may be that the MD08-3167 δD record

497 primarily reflects changes in the extent and position of the source region, with sediment being
498 primarily derived from the arid Namib region during periods of reduced wind strength, and from more
499 humid regions to the south when the wind field was stronger and more extensive. This scenario - which
500 could also determine the variability observed in other marine records from the Southeast Atlantic -
501 would provide a more comprehensive explanation for the variability observed in the MD08-3167
502 record, including the long-term decrease in δD values across the last glacial period and the relatively
503 high values during the Holocene (Figure 11), but the resolution of these questions remains a matter
504 for discussion and comparison with a fuller continental dataset.

505 [Inferences of climate variability in southern Africa based on orbital forcing](#)

506 Establishing a framework of climate change dynamics and environmental change in southern Africa is,
507 as mentioned, problematic, as so little evidence is available from the region. This paper establishes in
508 general terms, based on the records available, the climatic response to changes in earth's orbital
509 parameters with the goal of informing inferences of environmental change for periods and regions
510 where direct proxy evidence is not available.

511 At the broadest scale, it appears likely that southwestern and southeastern Africa have,
512 despite the same latitude, experienced markedly different environmental histories, and generally
513 respond to fundamentally different drivers. In southwestern Africa, SST records from SE Atlantic
514 marine cores (Etourneau et al., 2009; Marlow et al., 2000) closely mirror the variability observed in the
515 LR04 global benthic foraminifera $\delta^{18}O$ record (Lisiecki and Raymo, 2005), indicating that variability in
516 this system is closely tied to the development of high latitude ice sheets. A variety of proxy records
517 obtained from SE Atlantic marine cores spanning the last glacial-interglacial cycle have been
518 interpreted as indicating windier conditions associated with an intensified/displaced South Atlantic
519 anticyclone during phases of global cooling (Little et al., 1997; Pichevin et al., 2005; Stuut et al., 2002),
520 coupled with increased winter rainfall (Shi et al., 2001) and more humid conditions in southwestern
521 Africa (Stuut et al., 2004; Stuut et al., 2002). While the wind field and upwelling reconstructions appear
522 robust, inferences of changes in terrestrial environments have been shown to be more complicated,
523 with significant contradictions existing between marine (Collins et al., 2014; Shi et al., 2001) and
524 terrestrial records (Chase et al., 2019b; Lim et al., 2016; Scott et al., 2004). The best resolved terrestrial
525 records indicate that the last glacial period was generally more humid than the Holocene, but that
526 periods of increased upwelling – concurrent with lower boreal summer insolation – were relatively
527 arid, driven by the advection of cool, dry air from the Atlantic margin (Chase et al., 2019b). This
528 suggests that while changes in potential evapotranspiration play a significant role in determining
529 regional water balance (with cooler periods being generally more humid; Chase et al., 2019b; Lim et
530 al., 2016), precipitation exhibits a positive relationship with Benguela SSTs (Chase et al., 2015; Chase

531 et al., 2019b). This information can be applied to the SE Atlantic SST records to infer general patterns
532 of terrestrial environmental change along the western continental margin.

533 In southeastern Africa, at orbital timescales, precipitation variability is most clearly controlled
534 by changes in eccentricity and precession as they influence the amount and seasonality of direct
535 insolation. Significant correlations exist between proxy precipitation records and ~100-kyr, ~400-kyr
536 and perhaps even ~2400-kyr cycles of eccentricity (Caley et al., 2018; Johnson et al., 2016; Lyons et al.,
537 2015). This recognition sheds light on some previously confounding patterns, such as contextualising
538 the age distributions of the Cradle of Humankind flowstones, which the authors concluded could not
539 be easily explained by changes in insolation (Pickering et al., 2019). As described above, the Lake
540 Malawi region and Zambezi basin present an intriguing anomaly along an otherwise relatively
541 homogeneous climate response gradient spanning much of Africa's eastern margin (Chevalier and
542 Chase, 2015; Johnson et al., 2016; Schefuß et al., 2011; Wang et al., 2013). With this exception,
543 increased eccentricity generally results in increased rainfall/more humid conditions in the eastern
544 tropics. This relationship, however, apparently weakens during periods of reduced eccentricity and
545 higher global ice volume.

546 Based on these records and results, it may be suggested as a general guideline that under low
547 eccentricity ($< \sim 0.035$) and high global ice volume (LR04 $\delta^{18}\text{O}$ values $> \sim 4.3\text{‰}$), the influence of direct
548 forcing will decline and high latitude forcing may become more significant in the region (e.g. Figure 7).
549 As discussed above, the impact of this increased influence of high latitude forcing is apparent in the
550 breakdown of the positive relationship generally observed between precipitation and local summer
551 insolation at ~23-kyr precessional cycles (Chase et al., in press; Chevalier and Chase, 2015; Partridge et
552 al., 1997). These periods may have only occurred during the more intense glacial periods of the last
553 ~700-kyr, but precise thresholds are difficult to establish, as the available proxy records and associated
554 chronologies do not currently enable such exact refinement. These guideline values might, however,
555 serve as an indicator for when climate predictions based on local insolation values alone may become
556 less reliable.

557 The relationships and basic models described here have been defined using data obtained
558 primarily from the continental margins. While Lake Malawi and Tswaing Crater are located further
559 inland (~600 km and ~500 km respectively), no suitably resolved long records exist from the continental
560 interior (see Chase and Meadows, 2007; Singarayer and Burrough, 2015; Thomas and Burrough, 2012).
561 Records such as the MD08-3167 δD record (Collins et al., 2014) have been suggested to reflect
562 conditions closer to the interior, but its spatial and environmental significance has yet to be fully
563 resolved (Chase et al., 2019b; Collins et al., 2014; Singarayer and Burrough, 2015).

564 Over shorter timescales, considering finer-scale cycles and events, the relationships described
565 here become – or are apparently – more complex. It is clear that the available data pose many
566 questions that remain to be answered regarding the spatio-temporal nature of the observed anomalies
567 and their significance in the context of changes in the global climate system. It is concluded though
568 that the coupled consideration of orbital parameters and global boundary conditions and climate state
569 provides a useful – if general – indication of the potential of southern Africa’s diverse atmospheric and
570 oceanic circulation systems to influence regional environments. This may serve as a basis for both
571 refining ideas regarding the evolution of the region’s biodiversity and human history and enabling
572 more rigorous hypothesis testing for the role of climate variability as a driver of these processes.

573 Acknowledgements

574 I thank Tom Johnson, Andrew Carr, Lynne Quick, Manuel Chevalier, Martin Trauth, and three
575 anonymous reviewers for the constructive comments, input and perspective that have helped improve
576 this contribution. I also thank all of the researchers who have worked so hard to produce the datasets
577 and ideas considered in this paper.

578 References

- 579 Bajo, P., Drysdale, R.N., Woodhead, J.D., Hellstrom, J.C., Hodell, D., Ferretti, P., Voelker, A.H.L.,
580 Zanchetta, G., Rodrigues, T., Wolff, E., Tyler, J., Frisia, S., Spötl, C., Fallick, A.E., 2020. Persistent
581 influence of obliquity on ice age terminations since the Middle Pleistocene transition. *Science* 367,
582 1235-1239.
- 583 Batchelor, C.L., Margold, M., Krapp, M., Murton, D.K., Dalton, A.S., Gibbard, P.L., Stokes, C.R.,
584 Murton, J.B., Manica, A., 2019. The configuration of Northern Hemisphere ice sheets through the
585 Quaternary. *Nature Communications* 10, 3713.
- 586 Berger, A., Imbrie, J., Hays, J., Kukla, G., Saltzman, B., 1984. *Milankovitch and Climate*.
- 587 Bosmans, J.H.C., Hilgen, F.J., Tuenter, E., Lourens, L.J., 2015. Obliquity forcing of low-latitude climate.
588 *Clim. Past* 11, 1335-1346.
- 589 Boulila, S., Galbrun, B., Laskar, J., Pälike, H., 2012. A ~9myr cycle in Cenozoic $\delta^{13}\text{C}$ record and long-
590 term orbital eccentricity modulation: Is there a link? *Earth and Planetary Science Letters* 317-318,
591 273-281.
- 592 Braun, K., Bar-Matthews, M., Matthews, A., Ayalon, A., Cowling, R.M., Karkanas, P., Fisher, E.C., Dyez,
593 K., Zilberman, T., Marean, C.W., 2019. Late Pleistocene records of speleothem stable isotopic
594 compositions from Pinnacle Point on the South African south coast. *Quaternary Research* 91, 265-
595 288.
- 596 Braun, K., Bar-Matthews, M., Matthews, A., Ayalon, A., Zilberman, T., Cowling, R.M., Fisher, E.C.,
597 Herries, A.I.R., Brink, J.S., Marean, C.W., 2020. Comparison of climate and environment on the edge
598 of the Palaeo-Agulhas Plain to the Little Karoo (South Africa) in Marine Isotope Stages 5–3 as
599 indicated by speleothems. *Quaternary Science Reviews* 235, 105803.
- 600 Broecker, W.S., van Donk, J., 1970. Insolation changes, ice volumes, and the O^{18} record in deep-sea
601 cores. *Reviews of Geophysics* 8, 169-198.
- 602 Burrough, S.L., Thomas, D.S.G., Bailey, R.M., 2009. Mega-Lake in the Kalahari: a late Pleistocene
603 record of the Palaeolake Makgadikgadi system. *Quaternary Science Reviews* 28, 1392-1411.

604 Burrough, S.L., Thomas, D.S.G., Shaw, P.A., Bailey, R.M., 2007. Multiphase Quaternary highstands at
605 Lake Ngami, Kalahari, northern Botswana. *Palaeogeography, Palaeoclimatology, Palaeoecology* 253,
606 280-299.

607 Caley, T., Extier, T., Collins, J.A., Schefuß, E., Dupont, L., Malaizé, B., Rossignol, L., Souron, A.,
608 McClymont, E.L., Jimenez-Espejo, F.J., García-Comas, C., Eynaud, F., Martinez, P., Roche, D.M., Jorry,
609 S.J., Charlier, K., Wary, M., Gourves, P.-Y., Billy, I., Giraudeau, J., 2018. A two-million-year-long
610 hydroclimatic context for hominin evolution in southeastern Africa. *Nature* 560, 76-79.

611 Caley, T., Kim, J.H., Malaizé, B., Giraudeau, J., Laepple, T., Caillon, N., Charlier, K., Rebaubier, H.,
612 Rossignol, L., Castañeda, I.S., Schouten, S., Sinninghe Damsté, J.S., 2011. High-latitude obliquity as a
613 dominant forcing in the Agulhas current system. *Climates of the Past* 7, 1285-1296.

614 Castañeda, I.S., Caley, T., Dupont, L., Kim, J.-H., Malaizé, B., Schouten, S., 2016. Middle to Late
615 Pleistocene vegetation and climate change in subtropical southern East Africa. *Earth and Planetary
616 Science Letters* 450, 306-316.

617 Chappell, J., 1973. Astronomical theory of climatic change: status and problem. *Quaternary Research*
618 3, 221-236.

619 Chase, B., Harris, C., Wit, M.J.d., Kramers, J., Doel, S., Stankiewicz, J., in press. South African
620 speleothems reveal influence of high- and low latitude forcing over the last 113.5 kyr. *Geology*.

621 Chase, B.M., Boom, A., Carr, A.S., Carré, M., Chevalier, M., Meadows, M.E., Pedro, J.B., Stager, J.C.,
622 Reimer, P.J., 2015. Evolving southwest African response to abrupt deglacial North Atlantic climate
623 change events. *Quaternary Science Reviews* 121, 132-136.

624 Chase, B.M., Boom, A., Carr, A.S., Chevalier, M., Quick, L.J., Verboom, G.A., Reimer, P.J., 2019a.
625 Extreme hydroclimate response gradients within the western Cape Floristic region of South Africa
626 since the Last Glacial Maximum. *Quaternary Science Reviews* 219, 297-307.

627 Chase, B.M., Chevalier, M., Boom, A., Carr, A.S., 2017. The dynamic relationship between temperate
628 and tropical circulation systems across South Africa since the last glacial maximum. *Quaternary
629 Science Reviews* 174, 54-62.

630 Chase, B.M., Meadows, M.E., 2007. Late Quaternary dynamics of southern Africa's winter rainfall
631 zone. *Earth-Science Reviews* 84, 103-138.

632 Chase, B.M., Niedermeyer, E.M., Boom, A., Carr, A.S., Chevalier, M., He, F., Meadows, M.E., Ogle, N.,
633 Reimer, P.J., 2019b. Orbital controls on Namib Desert hydroclimate over the past 50,000 years.
634 *Geology*.

635 Chase, B.M., Quick, L.J., 2018. Influence of Agulhas forcing of Holocene climate change in South
636 Africa's southern Cape. *Quaternary Research* 90, 303-309.

637 Chase, B.M., Quick, L.J., Meadows, M.E., Scott, L., Thomas, D.S.G., Reimer, P.J., 2011. Late glacial
638 interhemispheric climate dynamics revealed in South African hyrax middens. *Geology* 39, 19-22.

639 Cheng, H., Edwards, R.L., Sinha, A., Spötl, C., Yi, L., Chen, S., Kelly, M., Kathayat, G., Wang, X., Li, X.,
640 Kong, X., Wang, Y., Ning, Y., Zhang, H., 2016. The Asian monsoon over the past 640,000 years and ice
641 age terminations. *Nature* 534, 640.

642 Chevalier, M., Brewer, S., Chase, B.M., 2017. Qualitative assessment of PMIP3 rainfall simulations
643 across the eastern African monsoon domains during the mid-Holocene and the Last Glacial
644 Maximum. *Quaternary Science Reviews* 156, 107--120.

645 Chevalier, M., Chase, B.M., 2015. Southeast African records reveal a coherent shift from high- to low-
646 latitude forcing mechanisms along the east African margin across last glacial–interglacial transition.
647 *Quaternary Science Reviews* 125, 117-130.

648 Chevalier, M., Chase, B.M., Quick, L.J., Dupont, L.M., Johnson, T.C., 2020. Temperature change in
649 subtropical southeastern Africa during the past 790,000 yr. *Geology*.

650 Clark, P.U., Archer, D., Pollard, D., Blum, J.D., Rial, J.A., Brovkin, V., Mix, A.C., Piasias, N.G., Roy, M.,
651 2006. The middle Pleistocene transition: characteristics, mechanisms, and implications for long-term
652 changes in atmospheric pCO₂. *Quaternary Science Reviews* 25, 3150-3184.

653 Cockcroft, M.J., Wilkinson, M.J., Tyson, P.D., 1987. The application of a present-day climatic model to
654 the late Quaternary in southern Africa. *Climatic Change* 10, 161-181.

655 Collins, J.A., Schefuß, E., Govin, A., Mulitza, S., Tiedemann, R., 2014. Insolation and glacial–interglacial
656 control on southwestern African hydroclimate over the past 140 000 years. *Earth and Planetary*
657 *Science Letters* 398, 1-10.

658 Cooper, G.R.J., Cowan, D.R., 2008. Comparing time series using wavelet-based semblance analysis.
659 *Computers & Geosciences* 34, 95-102.

660 Cordova, C.E., Scott, L., Chase, B.M., Chevalier, M., 2017. Late Pleistocene-Holocene vegetation and
661 climate change in the Middle Kalahari, Lake Ngami, Botswana. *Quaternary Science Reviews* 171, 199-
662 215.

663 Crampton, J.S., Meyers, S.R., Cooper, R.A., Sadler, P.M., Foote, M., Harte, D., 2018. Pacing of
664 Paleozoic macroevolutionary rates by Milankovitch grand cycles. *Proceedings of the National*
665 *Academy of Sciences* 115, 5686-5691.

666 Crétat, J., Pohl, B., Dieppois, B., Berthou, S., Pergaud, J., 2019. The Angola Low: relationship with
667 southern African rainfall and ENSO. *Climate Dynamics* 52, 1783-1803.

668 Crétat, J., Richard, Y., Pohl, B., Rouault, M., Reason, C., Fauchereau, N., 2012. Recurrent daily rainfall
669 patterns over South Africa and associated dynamics during the core of the austral summer.
670 *International Journal of Climatology* 32, 261-273.

671 Cruz Jr., F.W., Burns, S.J., Vuille, M., Karmann, I., Viana Jr., O., Sharp, W.D., Cardoso, A.O., Silva Dias,
672 P.L., Ferrari, J.A., 2005. Insolation-driven changes in atmospheric circulation over the past 116,000
673 years in subtropical Brazil. *Nature* 434, 63-66.

674 Dansgaard, W., 1964. Stable isotopes in precipitation. *Tellus* 16, 436-447.

675 de Boor, C., 2001. *A practical guide to splines*. Springer.

676 deMenocal, P.B., 1995. Plio-Pleistocene African climate. *Science* 270, 53-59.

677 Dupont, L.M., Caley, T., Castañeda, I.S., 2019. Effects of atmospheric CO₂ variability of the past 800
678 kyr on the biomes of southeast Africa. *Clim. Past* 15, 1083-1097.

679 Dupont, L.M., Caley, T., Kim, J.H., Castañeda, I., Malaizé, B., Giraudeau, J., 2011. Glacial-interglacial
680 vegetation dynamics in South Eastern Africa coupled to sea surface temperature variations in the
681 Western Indian Ocean. *Clim. Past* 7, 1209-1224.

682 Dupont, L.M., Kuhlmann, H., 2017. Glacial-interglacial vegetation change in the Zambezi catchment.
683 *Quaternary Science Reviews* 155, 127-135.

684 Engelbrecht, F.A., Marean, C.W., Cowling, R.M., Engelbrecht, C.J., Neumann, F.H., Scott, L., Nkoana,
685 R., O'Neal, D., Fisher, E., Shook, E., Franklin, J., Thatcher, M., McGregor, J.L., Van der Merwe, J.,
686 Dedekind, Z., Difford, M., 2019. Downscaling Last Glacial Maximum climate over southern Africa.
687 *Quaternary Science Reviews* 226, 105879.

688 Etourneau, J., Martinez, P., Blanz, T., Schneider, R., 2009. Pliocene-Pleistocene variability of upwelling
689 activity, productivity, and nutrient cycling in the Benguela region. *Geology* 37, 871-874.

690 Farmer, E.C., deMenocal, P.B., Marchitto, T.M., 2005. Holocene and deglacial ocean temperature
691 variability in the Benguela upwelling region: implications for low-latitude atmospheric circulation.
692 *Paleoceanography* 20, doi:10.1029/2004PA001049.

693 Gordon, C., Cooper, C., Senior, C.A., Banks, H., Gregory, J.M., Johns, T.C., Mitchell, J.F.B., Wood, R.A.,
694 2000. The simulation of SST, sea ice extents and ocean heat transports in a version of the Hadley
695 Centre coupled model without flux adjustments. *Climate Dynamics* 16, 147-168.

696 Grant, K.M., Rohling, E.J., Westerhold, T., Zabel, M., Heslop, D., Konijnendijk, T., Lourens, L., 2017. A 3
697 million year index for North African humidity/aridity and the implication of potential pan-African
698 Humid periods. *Quaternary Science Reviews* 171, 100-118.

699 Hays, J.D., Imbrie, J., Shackleton, N.J., 1976. Variations in the earth's orbit: pacemaker of the Ice
700 Ages. *Science* 194, 1121-1132.

701 Herrmann, N., Boom, A., Carr, A.S., Chase, B.M., West, A.G., Zabel, M., Schefuß, E., 2017. Hydrogen
702 isotope fractionation of leaf wax n-alkanes in southern African soils. *Organic Geochemistry* 109, 1-13.

703 Hijmans, R., Cameron, S.E., Parra, J.L., Jones, P.G., Jarvis, A., 2005. Very high resolution interpolated
704 climate surfaces for global land areas. *International Journal of Climatology* 25, 1965-1978.

705 Holmgren, K., Lee-Thorp, J.A., Cooper, G.R.J., Lundblad, K., Partridge, T.C., Scott, L., Sithaldeen, R.,
706 Talma, A.S., Tyson, P.D., 2003. Persistent millennial-scale climatic variability over the past 25,000
707 years in Southern Africa. *Quaternary Science Reviews* 22, 2311-2326.

708 Howard, E., Washington, R., 2019. Drylines in Southern Africa: Rediscovering the Congo Air Boundary.
709 *Journal of Climate* 32, 8223-8242.

710 Huybers, P., 2006. Early Pleistocene Glacial Cycles and the Integrated Summer Insolation Forcing.
711 *Science* 313, 508-511.

712 Huybers, P., 2011. Combined obliquity and precession pacing of late Pleistocene deglaciations.
713 *Nature* 480, 229-232.

714 Imbrie, J., 1982. Astronomical theory of the Pleistocene ice ages: a brief historical review. *Icarus* 50,
715 408-422.

716 Imbrie, J., Hays, J.D., Martinson, D.G., McIntyre, A., Mix, A.C., Morley, J.J., Pisias, N.G., Prell, W.L.,
717 Shackleton, N.J., 1984. The orbital theory of Pleistocene climate: support from a revised chronology
718 of the marine $\delta^{18}\text{O}$ record, in: Berger, A., Imbrie, J., Hays, J., Kukla, G., Saltzman, B. (Eds.),
719 *Milankovitch and Climate, Part 1*. Reidel Publishing Co., Dordrecht, pp. 269-305.

720 Ivory, S.J., Lézine, A.-M., Vincens, A., Cohen, A.S., 2018. Waxing and waning of forests: Late
721 Quaternary biogeography of southeast Africa. *Global Change Biology* 24, 2939-2951.

722 Johnson, T.C., Werne, J.P., Brown, E.T., Abbott, A., Berke, M., Steinman, B.A., Halbur, J., Contreras, S.,
723 Grosshuesch, S., Deino, A., Scholz, C.A., Lyons, R.P., Schouten, S., Damsté, J.S.S., 2016. A progressively
724 wetter climate in southern East Africa over the past 1.3 million years. *Nature* 537, 220-224.

725 Koutsodendris, A., Nakajima, K., Kaboth-Bahr, S., Berke, M.A., Franzese, A.M., Hall, I.R., Hemming,
726 S.R., Just, J., LeVay, L.J., Pross, J., Robinson, R., 2021. A Plio-Pleistocene (c. 0–4 Ma) cyclostratigraphy
727 for IODP Site U1478 (Mozambique Channel, SW Indian Ocean): Exploring an offshore record of
728 paleoclimate and ecosystem variability in SE Africa. *Newsletters on Stratigraphy* 54, 159-181.

729 Kutzbach, J.E., 1981. Monsoon climate of the early Holocene: climate experiment with the Earth's
730 orbital parameters for 9000 years ago. *Science* 214, 59-61.

731 Kutzbach, J.E., Guan, J., He, F., Cohen, A.S., Orland, I.J., Chen, G., 2020. African climate response to
732 orbital and glacial forcing in 140,000-y simulation with implications for early modern human
733 environments. *Proceedings of the National Academy of Sciences*, 201917673.

734 Laskar, J., Robutel, P., Joutel, F., Gastineau, M., Correia, A.C.M., Levrard, B., 2004. A long-term
735 numerical solution for the insolation quantities of the Earth. *A&A* 428, 261-285.

736 Lim, S., Chase, B.M., Chevalier, M., Reimer, P.J., 2016. 50,000 years of vegetation and climate change
737 in the southern Namib Desert, Pella, South Africa. *Palaeogeography, Palaeoclimatology,*
738 *Palaeoecology* 451, 197-209.

739 Lisiecki, L.E., Raymo, M.E., 2005. A Pliocene-Pleistocene stack of 57 globally distributed benthic $\delta^{18}\text{O}$
740 records. *Paleoceanography* 20, PA1003.

741 Little, M.G., Schneider, R.R., Kroon, D., Price, B., Bickert, T., Wefer, G., 1997. Rapid
742 palaeoceanographic changes in the Benguela Upwelling System for the last 160,000 years as
743 indicated by abundances of planktonic foraminifera. *Palaeogeography, Palaeoclimatology,*
744 *Palaeoecology* 130, 135-161.

745 Lyons, R.P., Scholz, C.A., Cohen, A.S., King, J.W., Brown, E.T., Ivory, S.J., Johnson, T.C., Deino, A.L.,
746 Reinthal, P.N., McGlue, M.M., Blome, M.W., 2015. Continuous 1.3-million-year record of East African
747 hydroclimate, and implications for patterns of evolution and biodiversity. *Proceedings of the National*
748 *Academy of Sciences* 112, 15568-15573.

749 Marlow, J.R., Lange, C.B., Wefer, G., Rosell-Mele, A., 2000. Upwelling intensification as part of the
750 Pliocene-Pleistocene climate transition. *Science* 290, 2288-2291.

751 Milankovitch, M.K., 1930. *Mathematische Klimalehre und Astronomische Theorie der*
752 *Klirnaschwankungen*. Gebruder Borntraeger, Berlin.

753 Mudelsee, M., Schulz, M., 1997. The Mid-Pleistocene climate transition: onset of 100 ka cycle lags ice
754 volume build-up by 280 ka. *Earth and Planetary Science Letters* 151, 117-123.

755 Nicholson, S.E., Entekhabi, D., 1987. Rainfall variability in equatorial and southern Africa:
756 relationships with sea surface temperatures along the southwestern coast of Africa. *Journal of*
757 *Climate and Applied Meteorology* 26, 561-578.

758 Nicholson, S.L., Pike, A.W.G., Hosfield, R., Roberts, N., Sahy, D., Woodhead, J., Cheng, H., Edwards,
759 R.L., Affolter, S., Leuenberger, M., Burns, S.J., Matter, A., Fleitmann, D., 2020. Pluvial periods in
760 Southern Arabia over the last 1.1 million-years. *Quaternary Science Reviews* 229, 106112.

761 Olsen, P.E., Kent, D.V., 1996. Milankovitch climate forcing in the tropics of Pangaea during the Late
762 Triassic. *Palaeogeography, Palaeoclimatology, Palaeoecology* 122, 1-26.

763 Otto-Bliesner, B.L., Russell, J.M., Clark, P.U., Liu, Z., Overpeck, J.T., Konecky, B., deMenocal, P.,
764 Nicholson, S.E., He, F., Lu, Z., 2014. Coherent changes of southeastern equatorial and northern
765 African rainfall during the last deglaciation. *Science* 346, 1223-1227.

766 Owen, R.B., Muiruri, V.M., Lowenstein, T.K., Renaut, R.W., Rabideaux, N., Luo, S., Deino, A.L., Sier,
767 M.J., Dupont-Nivet, G., McNulty, E.P., Leet, K., Cohen, A., Campisano, C., Deocampo, D., Shen, C.-C.,
768 Billingsley, A., Mbuthia, A., 2018. Progressive aridification in East Africa over the last half million
769 years and implications for human evolution. *Proceedings of the National Academy of Sciences* 115,
770 11174-11179.

771 Pälike, H., Frazier, J., Zachos, J.C., 2006a. Extended orbitally forced palaeoclimatic records from the
772 equatorial Atlantic Ceara Rise. *Quaternary Science Reviews* 25, 3138-3149.

773 Pälike, H., Norris, R.D., Herrle, J.O., Wilson, P.A., Coxall, H.K., Lear, C.H., Shackleton, N.J., Tripathi, A.K.,
774 Wade, B.S., 2006b. The Heartbeat of the Oligocene Climate System. *Science* 314, 1894-1898.

775 Partridge, T.C., deMenocal, P.B., Lorentz, S.A., Paiker, M.J., Vogel, J.C., 1997. Orbital forcing of
776 climate over South Africa: a 200,000-year rainfall record from the Pretoria Saltpan. *Quaternary*
777 *Science Reviews* 16, 1125-1133.

778 Peel, M.C., Finlayson, B.L., McMahon, T.A., 2007. Updated world map of the Köppen-Geiger climate
779 classification. *Hydrol. Earth Syst. Sci.* 11, 1633-1644.

780 Peeters, F.J.C., Acheson, R., Brummer, G.-J.A., de Ruijter, W.P.M., Schneider, R.R., Ganssen, G.M.,
781 Ufkes, E., Kroon, D., 2004. Vigorous exchange between the Indian and Atlantic oceans at the end of
782 the past five glacial periods. *Nature* 430, 661-665.

783 Pichevin, L., Cremer, M., Giraudeau, J., Bertrand, P., 2005. A 190 kyr record of lithogenic grain-size on
784 the Namibian slope: forging a tight link between past wind-strength and coastal upwelling dynamics.
785 *Marine Geology* 218, 81-96.

786 Pickering, R., Herries, A.I.R., Woodhead, J.D., Hellstrom, J.C., Green, H.E., Paul, B., Ritzman, T., Strait,
787 D.S., Schoville, B.J., Hancox, P.J., 2019. U–Pb-dated flowstones restrict South African early hominin
788 record to dry climate phases. *Nature* 565, 226-229.

789 Pope, V.D., Gallani, M.L., Rowntree, P.R., Stratton, R.A., 2000. The impact of new physical
790 parametrizations in the Hadley Centre climate model: HadAM3. *Climate Dynamics* 16, 123-146.

791 Ravelo, A.C., Andreasen, D.H., Lyle, M., Olivarez Lyle, A., Wara, M.W., 2004. Regional climate shifts
792 caused by gradual global cooling in the Pliocene epoch. *Nature* 429, 263-267.

793 Reason, C.J.C., Rouault, M., Melice, J.L., Jagadheesha, D., 2002. Interannual winter rainfall variability
794 in SW South Africa and large scale ocean–atmosphere interactions. *Meteorology and Atmospheric*
795 *Physics* 80, 19-29.

796 Rossignol-Strick, M., 1983. African monsoon, an immediate climate response to orbital insolation.
797 *Nature* 304, 46-49.

798 Rouault, M., Florenchie, P., Fauchereau, N., Reason, C.J.C., 2003. South East tropical Atlantic warm
799 events and southern African rainfall. *Geophysical Research Letters* 30.

800 Rouault, M., White, S.A., Reason, C.J.C., Lutjeharms, J.R.E., Jobard, I., 2002. Ocean–Atmosphere
801 Interaction in the Agulhas Current Region and a South African Extreme Weather Event. *Weather &*
802 *Forecasting* 17, 655.

803 Ruddiman, W.F., 2006a. Orbital changes and climate. *Quaternary Science Reviews* 25, 3092-3112.

804 Ruddiman, W.F., 2006b. What is the timing of orbital-scale monsoon changes? *Quaternary Science*
805 *Reviews* 25, 657-658.

806 Schefuß, E., Kuhlmann, H., Mollenhauer, G., Prange, M., Pätzold, J., 2011. Forcing of wet phases in
807 southeast Africa over the past 17,000 years. *Nature* 480, 509-512.

808 Schmidt, G.A., Kelley, M., Nazarenko, L., Ruedy, R., Russell, G.L., Aleinov, I., Bauer, M., Bauer, S.E.,
809 Bhat, M.K., Bleck, R., Canuto, V., Chen, Y.-H., Cheng, Y., Clune, T.L., Del Genio, A., de Fainchtein, R.,
810 Faluvegi, G., Hansen, J.E., Healy, R.J., Kiang, N.Y., Koch, D., Lacis, A.A., LeGrande, A.N., Lerner, J., Lo,
811 K.K., Matthews, E.E., Menon, S., Miller, R.L., Oinas, V., Oloso, A.O., Perlwitz, J.P., Puma, M.J., Putman,
812 W.M., Rind, D., Romanou, A., Sato, M., Shindell, D.T., Sun, S., Syed, R.A., Tausnev, N., Tsigaridis, K.,
813 Unger, N., Voulgarakis, A., Yao, M.-S., Zhang, J., 2014. Configuration and assessment of the GISS
814 ModelE2 contributions to the CMIP5 archive. *Journal of Advances in Modeling Earth Systems* 6, 141-
815 184.

816 Scholz, C.A., Johnson, T.C., Cohen, A.S., King, J.W., Peck, J.A., Overpeck, J.T., Talbot, M.R., Brown, E.T.,
817 Kalindekaffe, L., Amoako, P.Y.O., Lyons, R.P., Shanahan, T.M., Castaneda, I.S., Heil, C.W., Forman, S.L.,
818 McHargue, L.R., Beuning, K.R., Gomez, J., Pierson, J., 2007. East African megadroughts between 135
819 and 75 thousand years ago and bearing on early-modern human origins. *Proceedings of the National
820 Academy of Sciences* 104, 16416-16421.

821 Scott, L., Marais, E., Brook, G.A., 2004. Fossil hyrax dung and evidence of Late Pleistocene and
822 Holocene vegetation types in the Namib Desert. *Journal of Quaternary Science* 19, 829-832.

823 Shi, N., Schneider, R., Beug, H.-J., Dupont, L.M., 2001. Southeast trade wind variations during the last
824 135 kyr: evidence from pollen spectra in eastern South Atlantic sediments. *Earth and Planetary
825 Science Letters* 187, 311-321.

826 Simon, M.H., Ziegler, M., Bosmans, J., Barker, S., Reason, C.J.C., Hall, I.R., 2015. Eastern South African
827 hydroclimate over the past 270,000 years. *Scientific Reports* 5, 18153.

828 Singarayer, J.S., Burrough, S.L., 2015. Interhemispheric dynamics of the African rainbelt during the
829 late Quaternary. *Quaternary Science Reviews* 124, 48-67.

830 Singarayer, J.S., Valdes, P.J., 2010. High-latitude climate sensitivity to ice-sheet forcing over the last
831 120kyr. *Quaternary Science Reviews* 29, 43-55.

832 Street-Perrott, F.A., Mitchell, J.F.B., Marchand, D.S., Brunner, J.S., 1990. Milankovitch and albedo
833 forcing of the tropical monsoons: a comparison of geological evidence and numerical simulations for
834 9000 BP. *Transactions - Royal Society of Edinburgh: Earth Sciences* 81, 407-427.

835 Stuut, J.-B.W., Crosta, X., van der Borg, K., Schneider, R., 2004. Relationship between Antarctic sea ice
836 and southwest African climate during the late Quaternary. *Geology* 32, 909-912.

837 Stuut, J.-B.W., Lamy, F., 2004. Climate variability at the southern boundaries of the Namib
838 (southwestern Africa) and Atacama (northern Chile) coastal deserts during the last 120,000 yr.
839 *Quaternary Research* 62, 301-309.

840 Stuut, J.-B.W., Prins, M.A., Schneider, R.R., Weltje, G.J., Jansen, J.H.F., Postma, G., 2002. A 300 kyr
841 record of aridity and wind strength in southwestern Africa: inferences from grain-size distributions of
842 sediments on Walvis Ridge, SE Atlantic. *Marine Geology* 180, 221-233.

843 Sueyoshi, T., Ohgaito, R., Yamamoto, A., Chikamoto, M.O., Hajima, T., Okajima, H., Yoshimori, M.,
844 Abe, M., O'Ishi, R., Saito, F., Watanabe, S., Kawamiya, M., Abe-Ouchi, A., 2013. Set-up of the PMIP3
845 paleoclimate experiments conducted using an Earth system model, MIROC-ESM. *Geosci. Model Dev.*
846 6, 819-836.

847 Talma, A.S., Vogel, J.C., 1992. Late Quaternary paleotemperatures derived from a speleothem from
848 Cango Caves, Cape Province, South Africa. *Quaternary Research* 37, 203-213.

849 Taylor, A.K., Berke, M.A., Castañeda, I.S., Koutsodendris, A., Campos, H., Hall, I.R., Hemming, S.R.,
850 LeVay, L.J., Sierra, A.C., O'Connor, K., Scientists, t.E., in press. Plio-Pleistocene Continental
851 Hydroclimate and Indian Ocean Sea Surface Temperatures at the Southeast African Margin.
852 *Paleoceanography and Paleoclimatology* n/a, e2020PA004186.

853 Thomas, D.S.G., Burrough, S.L., 2012. Interpreting geoproxies of late Quaternary climate change in
854 African drylands: implications for understanding environmental change and early human behaviour.
855 *Quaternary International* 253, 5-17.

856 Thomas, D.S.G., Shaw, P.A., 2002. Late Quaternary environmental change in central southern Africa:
857 new data, synthesis, issues and prospects. *Quaternary Science Reviews* 21, 783-797.

858 Tiedemann, R., Sarnthein, M., Shackleton, N.J., 1994. Astronomic timescale for the Pliocene Atlantic
859 $\delta^{18}O$ and dust flux records of Ocean Drilling Program Site 659. *Paleoceanography* 9, 619-638.
860 Tierney, J.E., deMenocal, P.B., Zander, P.D., 2017. A climatic context for the out-of-Africa migration.
861 *Geology* 45, 1023-1026.
862 Tierney, J.E., Russell, J.M., Huang, Y., Sinninghe Damsté, J.S., Hopmans, E.C., Cohen, A.S., 2008.
863 Northern Hemisphere controls on tropical southeast African climate during the past 60,000 years.
864 *Science* 322, 252-255.
865 Trauth, M.H., Larrasoana, J.C., Mudelsee, M., 2009. Trends, rhythms and events in Plio-Pleistocene
866 African climate. *Quaternary Science Reviews* 28, 399-411.
867 Tyson, P.D., 1986. *Climatic Change and Variability in Southern Africa*. Oxford University Press, Cape
868 Town.
869 Tyson, P.D., Preston-Whyte, R.A., 2000. *The Weather and Climate of Southern Africa*. Oxford
870 University Press, Cape Town.
871 Tzedakis, P.C., Crucifix, M., Mitsui, T., Wolff, E.W., 2017. A simple rule to determine which insolation
872 cycles lead to interglacials. *Nature* 542, 427-432.
873 van Zinderen Bakker, E.M., 1967. Upper Pleistocene stratigraphy and Holocene ecology on the basis
874 of vegetation changes in Sub-Saharan Africa, in: Bishop, W.W., Clark, J.D. (Eds.), *Background to*
875 *Evolution in Africa*. University of Chicago Press, Chicago, pp. 125-147.
876 van Zinderen Bakker, E.M., 1976. The evolution of late Quaternary paleoclimates of Southern Africa.
877 *Palaeoecology of Africa* 9, 160-202.
878 Vickery, K.J., Eckardt, F.D., Bryant, R.G., 2013. A sub-basin scale dust plume source frequency
879 inventory for southern Africa, 2005-2008. *Geophysical Research Letters* 40, 5274-5279.
880 Wang, B., Ding, Q., 2008. Global monsoon: dominant mode of annual variation in the tropics.
881 *Dynamics of Atmospheres and Oceans* 44, 165-183.
882 Wang, Y., Jian, Z., Zhao, P., Chen, J., Xiao, D., 2015. Precessional forced evolution of the Indian Ocean
883 Dipole. *Journal of Geophysical Research: Oceans* 120, 3747-3760.
884 Wang, Y.V., Larsen, T., Leduc, G., Andersen, N., Blanz, T., Schneider, R.R., 2013. What does leaf wax
885 δD from a mixed C3/C4 vegetation region tell us? *Geochimica et Cosmochimica Acta* 111, 128-139.

886

887

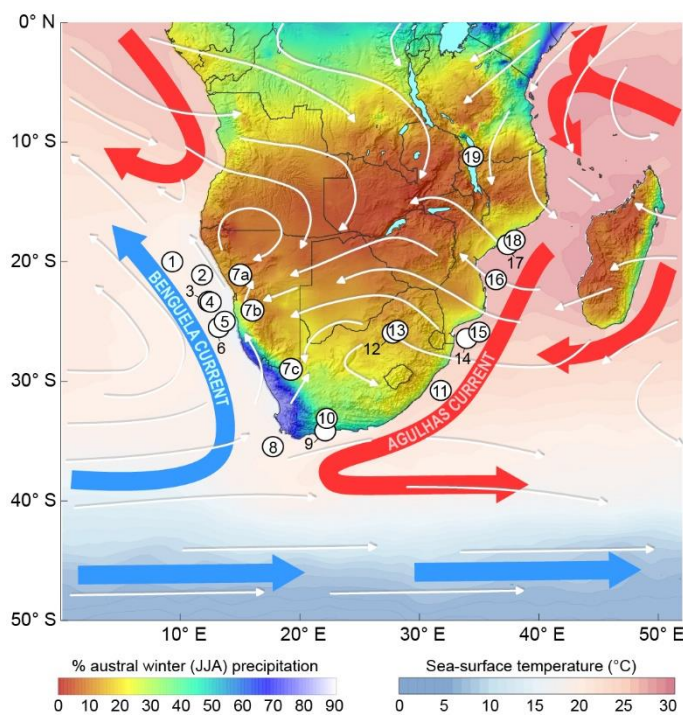


Figure 1: Map of southern Africa with primary atmospheric (white arrows) and oceanic circulation systems (blue arrows or cold currents, red arrows for warm currents) indicated. Terrestrial colour gradient indicates seasonal distribution of precipitation, with reds (blues) indicating a dominance of austral summer (winter) rainfall linked to tropical (temperate) moisture-bearing systems. Sites discussed are indicated by numbered dots as follows:

(1) MD96-2094 (Stuut et al., 2002); **(2)** ODP 1082 (Etourneau et al., 2009); **(3)** MD08-3167 (Collins et al., 2014); **(4)** GeoB 1711-4 (Little et al., 1997; Shi et al., 2001) **(5)** MD96-2087 (Pichevin et al., 2005); **(6)** ODP 1084 (Marlow et al., 2000); **(7a-c)** Namib Desert rock hyrax middens (Chase et al., 2019b); **(8)** MD96-2081 (Peeters et al., 2004); **(9)** Pinnacle Point (Braun et al., 2019); **(10)** Cango and Efflux caves (Braun et al., 2020; Chase et al., in press; Talma and Vogel, 1992); **(11)** CD154-10-06P (Simon et al., 2015); **(12)** Cradle of Humankind; **(13)** Tswaing Crater (Partridge et al., 1997); **(14)** MD96-2048 (Braun et al., 2020; Caley et al., 2018; Caley et al., 2011; Castañeda et al., 2016; Dupont et al., 2011); **(15)** ODP U1478 (Taylor et al., in press); **(16)** GeoB 9311-1 (Dupont and Kuhlmann, 2017); **(17)** GeoB 9307-3 (Schefuß et al., 2011); **(18)** GIK 16160-3 (Wang et al., 2013); **(19)** Lake Malawi (Johnson et al., 2016; Lyons et al., 2015).

911

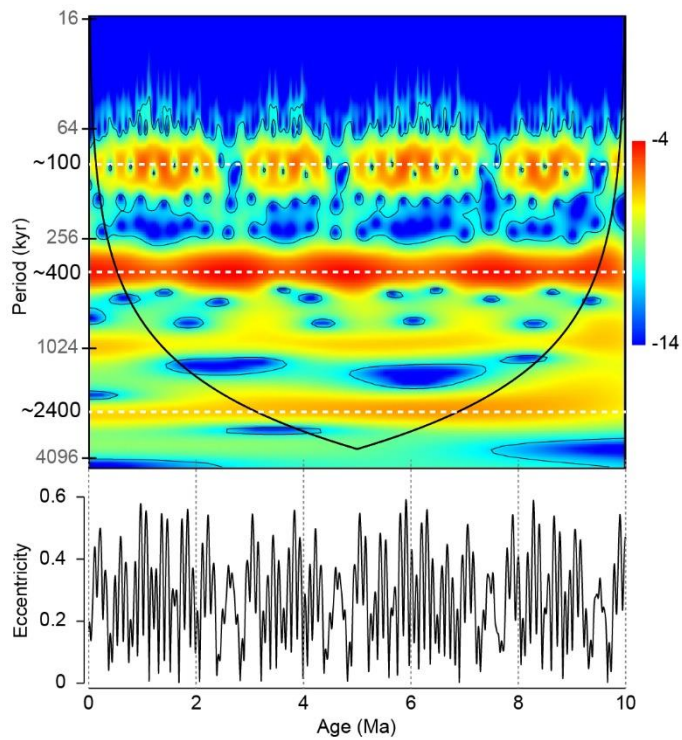


Figure 2: Power spectrum from continuous Morlet wavelet transform of 10 Myr orbital eccentricity data (Laskar et al., 2004). The cone of influence indicates the region beyond which there is potential for edge effects. The colour gradient indicates wavelet power (red = stronger signal), and the position of ~100-kyr, ~400-kyr and ~2400-kyr eccentricity cycles are highlighted by white dashed lines.

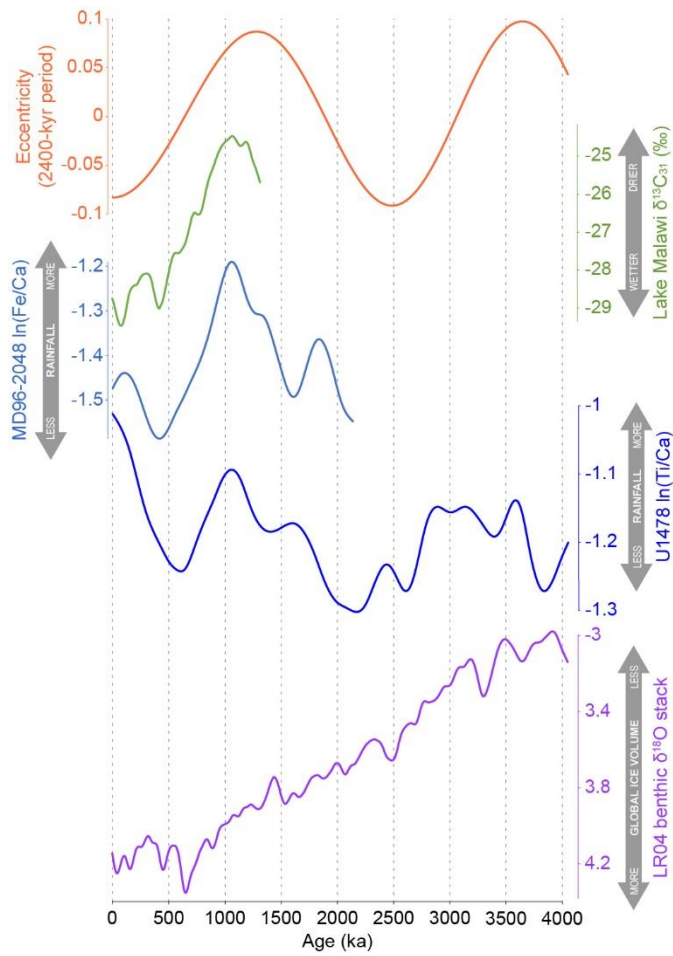


Figure 3: The ~2400-kyr orbital eccentricity cycle and records interpreted as indicators environmental variability from Lake Malawi (Johnson et al., 2016) and marine cores MD96-2048 (Caley et al., 2018) and Site U1478 (Koutsodendris et al., 2021) as well as the LR04 global benthic $\delta^{18}\text{O}$ record (Lisiecki and Raymo, 2005). The proxy records were smoothed to distil comparable signals using smoothing splines according to the algorithm of de Boor (2001).

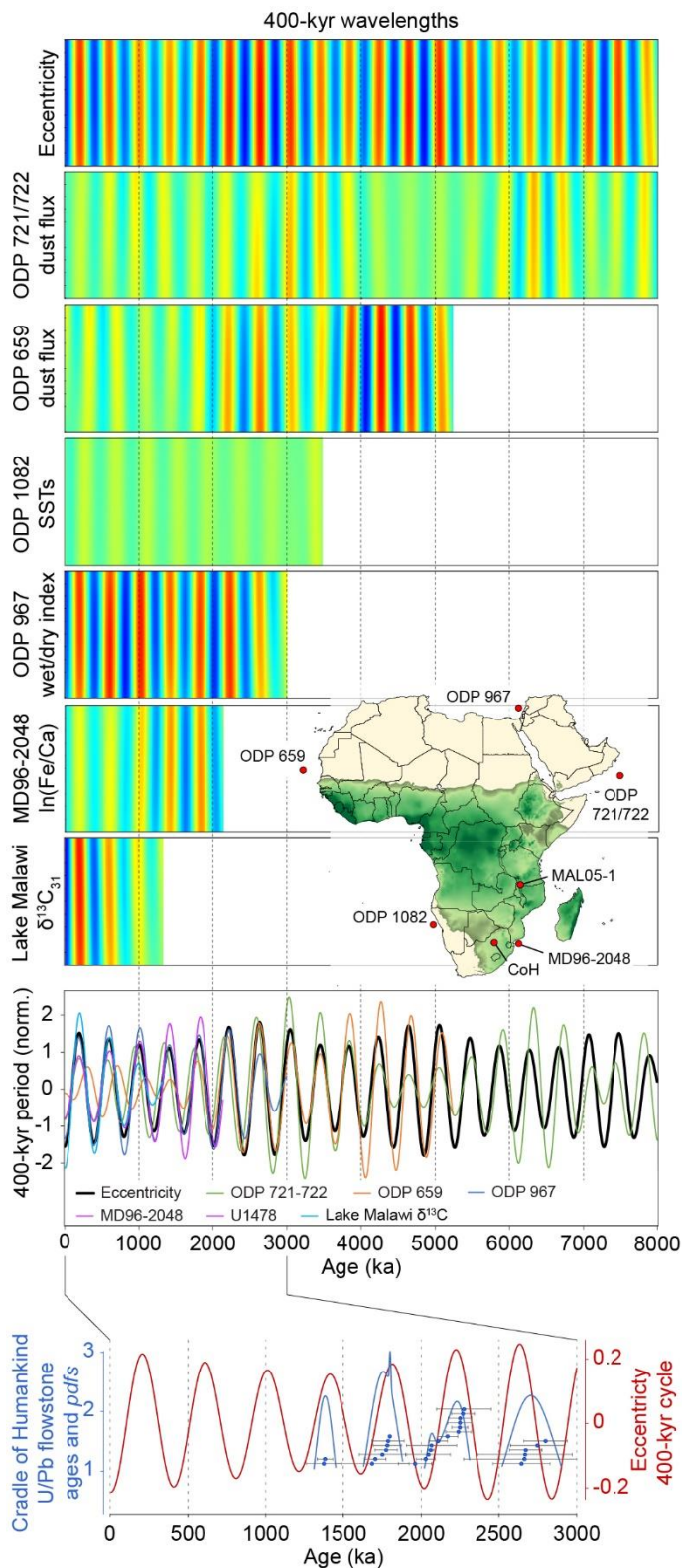
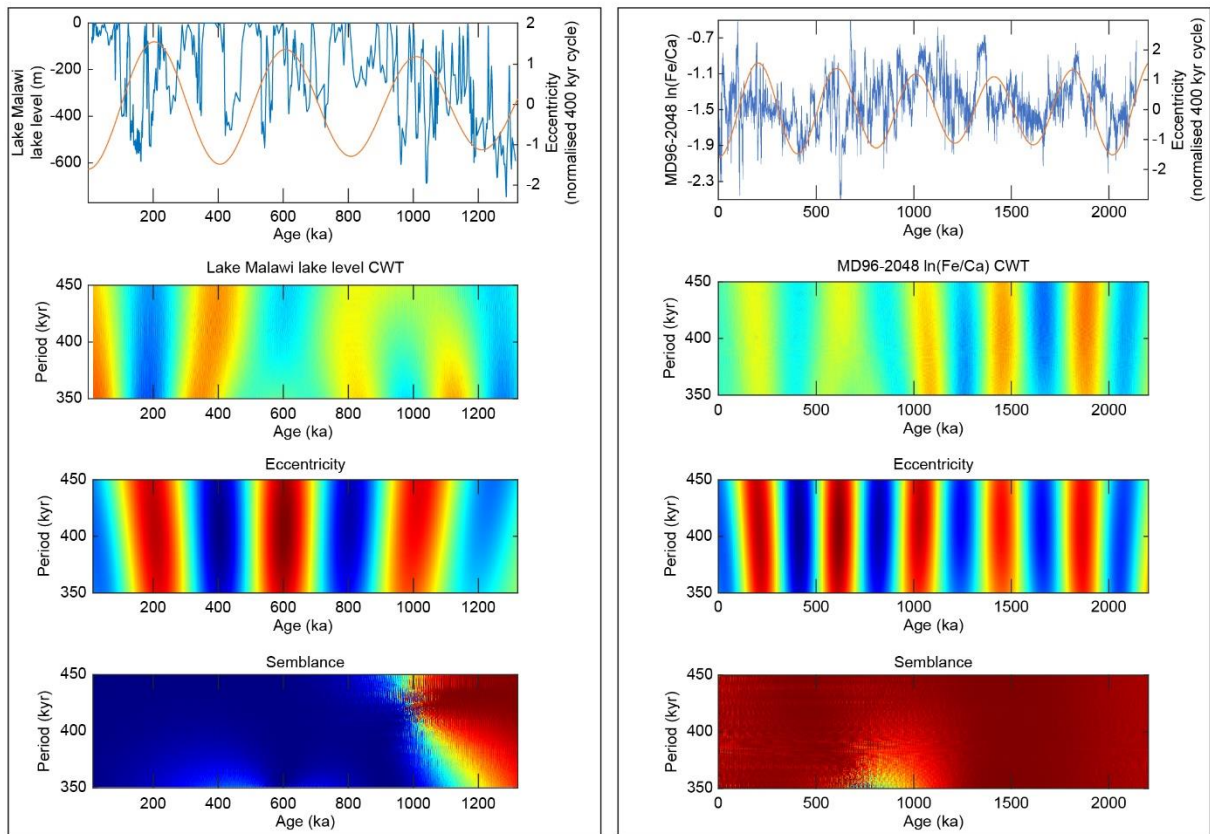


Figure 4: Comparison of real-value wavelet power spectra at 400-kyr periods from continuous Morlet wavelet transforms of: 1) orbital eccentricity data (Laskar et al., 2004), 2) ODP 721/722 dust flux data (deMenocal, 1995), 3) ODP 659 dust flux data (Tiedemann et al., 1994), 4) ODP 967 wet/dry index (Grant et al., 2017), 5) MD96-2048 $\ln(\text{Fe}/\text{Ca})$ data (Caley et al., 2018), and 6) Lake Malawi (MAL05-1) lake level reconstruction (Lyons et al., 2015). The colour gradient indicates real-value wavelet power (red indicates large positive anomalies while blue indicates large negative anomalies). The timing of the derived 400-kyr cycles is normalised (standard score) and compared to assess their phasing. The ~ 400 -kyr eccentricity cycle is compared to ages and probability density functions from the Cradle of Humankind (CoH) flowstones (Pickering et al., 2019). Map indicates location of sites considered, and in green the extent of the African tropical rainbelt (data from Hijmans et al., 2005; calculated according to Wang and Ding, 2008).



964

965 **Figure 5:** Semblance analysis (Cooper and Cowan, 2008) of Lake Malawi lake level data (Lyons et al.,
 966 2015) and MD96-2048 ln(Fe/Ca) data (Caley et al., 2018) with orbital eccentricity data (Laskar et al.,
 967 2004). Middle panes indicate real-value wavelet power of proxy records and eccentricity at ~400-kyr
 968 periods (red indicates large positive anomalies while blue indicates large negative anomalies). In the
 969 lower semblance pane, red indicates a semblance of +1 (positive correlation), and blue indicates a
 970 semblance of -1 (negative correlation).

971

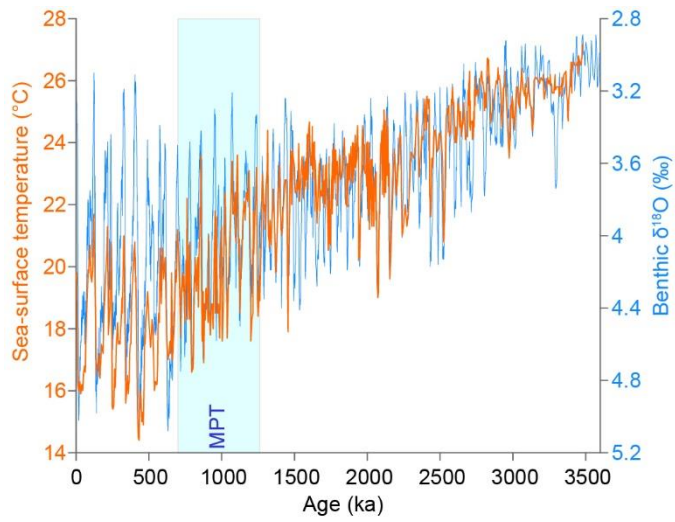
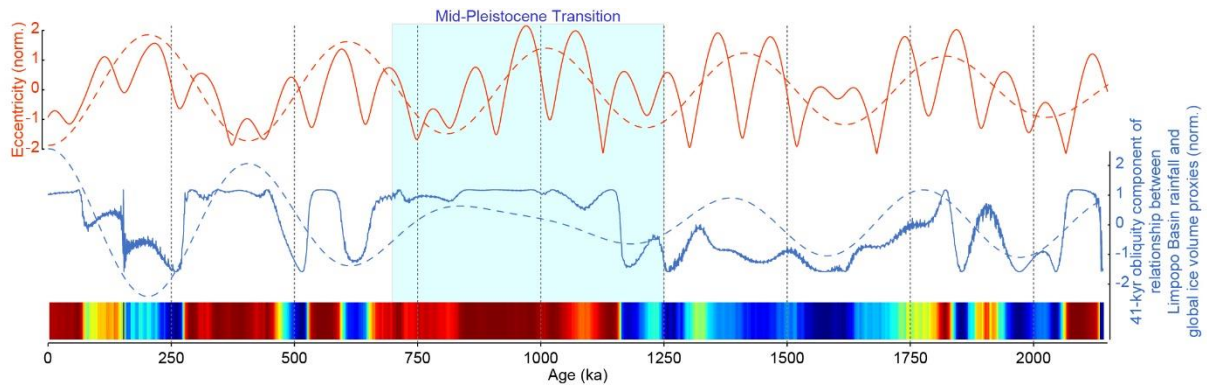


Figure 6: Comparison of the LR04 global benthic $\delta^{18}\text{O}$ record (Lisiecki and Raymo, 2005) with the ODP 1082 sea-surface temperature record from the Benguela upwelling system (Etourneau et al., 2009). Timing of the mid-Pleistocene transition (MPT; as per Clark et al., 2006) is indicated.



980

981 **Figure 7:** Comparison of 1) orbital eccentricity (orange lines; Laskar et al., 2004) with dashed line
 982 showing 400-kyr cycle, and 2) 41-kyr obliquity component from semblance analysis (blue lines and heat
 983 map, with 400-kyr filter depicted as dashed line; Cooper and Cowan, 2008) of the MD96-2048 $\ln(\text{Fe}/\text{Ca})$
 984 record, interpreted as reflecting changes in terrestrial sediment flux as a function of changes in rainfall
 985 amount in the Limpopo Basin (Caley et al., 2018) and the LR04 benthic $\delta^{18}\text{O}$ record reflecting changes
 986 in global ice volume (Lisiecki and Raymo, 2005). Semblance results (in heat map red=positive
 987 correlation and blue= negative correlation) indicate the response of Limpopo Basin to changes in global
 988 ice volume associated with variations in obliquity. Positive (negative) values indicate increased
 989 (decreased) sediment flux during phases of increased ice volume and decreased axial tilt. Prior to the
 990 mid-Pleistocene transition (MPT), a negative relationship generally exists between runoff and
 991 obliquity. Following the MPT, primarily during periods of low eccentricity and weakened low latitude
 992 forcing, runoff appears to increase during glacial periods.

993

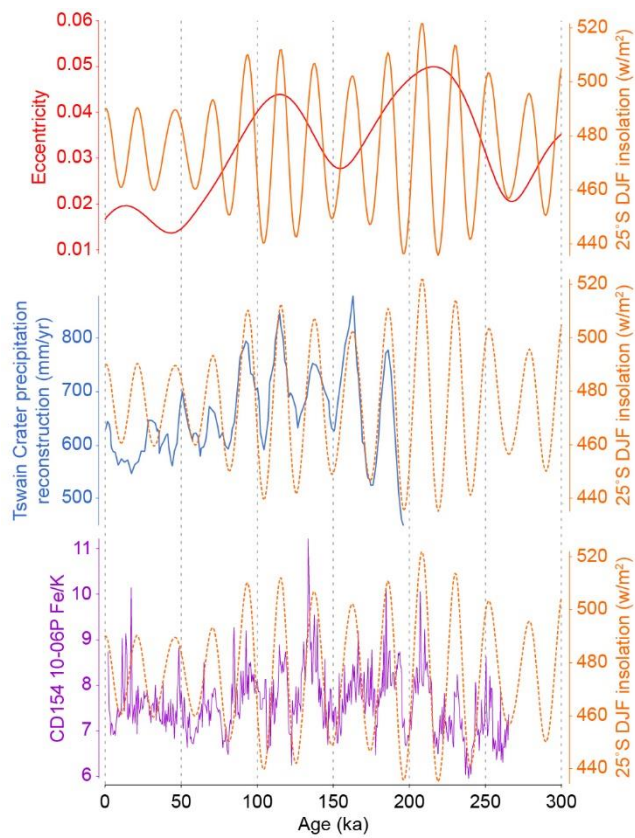
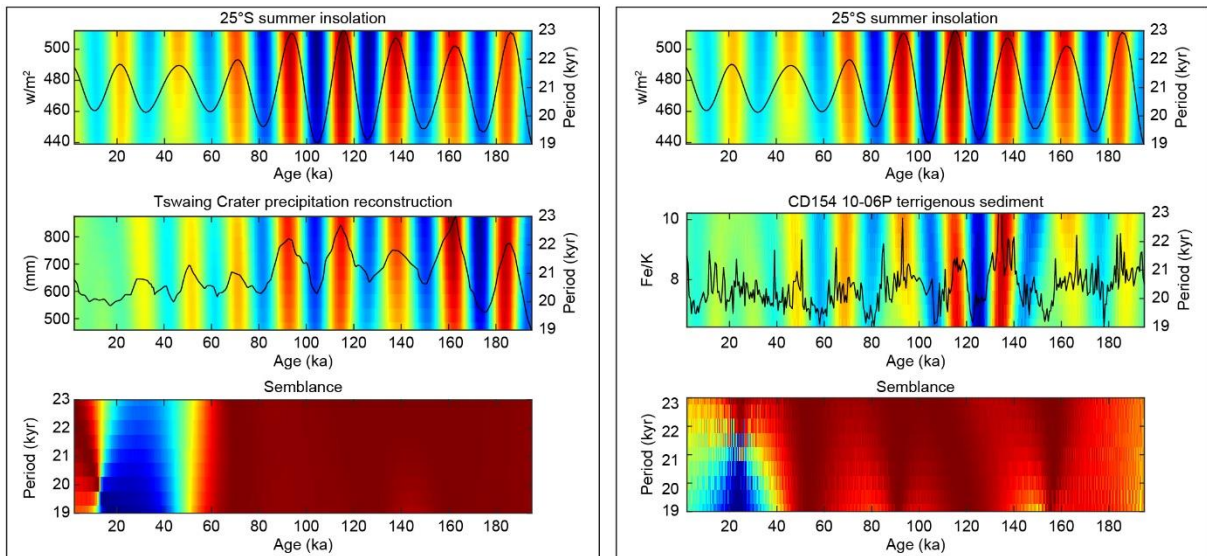


Figure 8: Orbital eccentricity and austral summer (DJF) insolation at 25°S (Laskar et al., 2004), and comparisons of summer insolation variability with the Tsuain Crater precipitation reconstruction (Partridge et al., 1997) and the CD154 10-06P Fe/K record (Simon et al., 2015).



1002

1003

Figure 9: Semblance analysis (Cooper and Cowan, 2008) of austral summer (DJF) insolation at 25°S (Laskar et al., 2004), the Tswaing Crater precipitation reconstruction (Partridge et al., 1997) and the CD154 10-06P Fe/K record (Simon et al., 2015). Colour in upper panes indicate real-value signal power (red indicates large positive anomalies whereas blue indicates large negative anomalies), whereas in the lower semblance pane, red indicates a semblance of +1 (positive correlation), and blue indicates a semblance of -1 (negative correlation).

1009

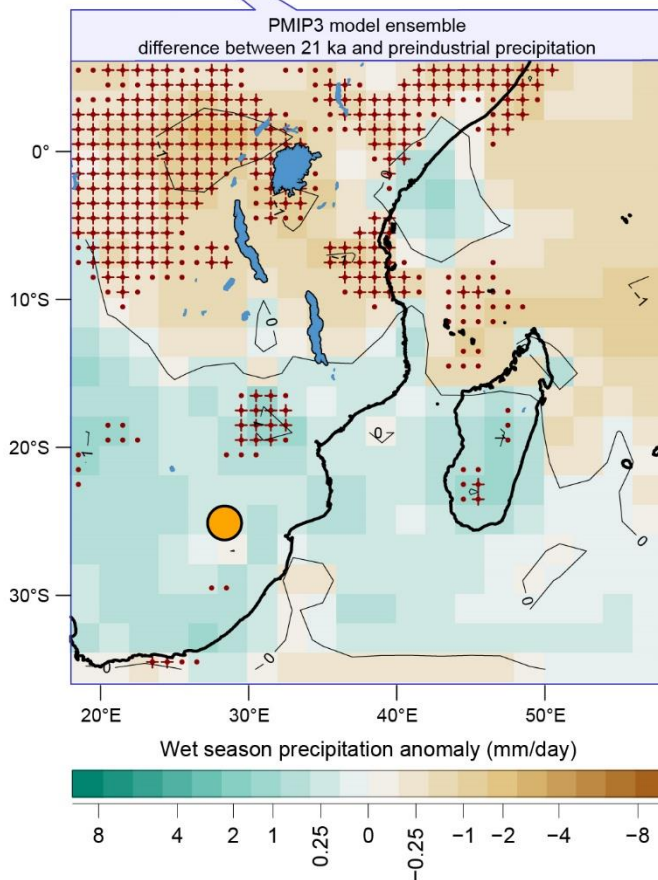
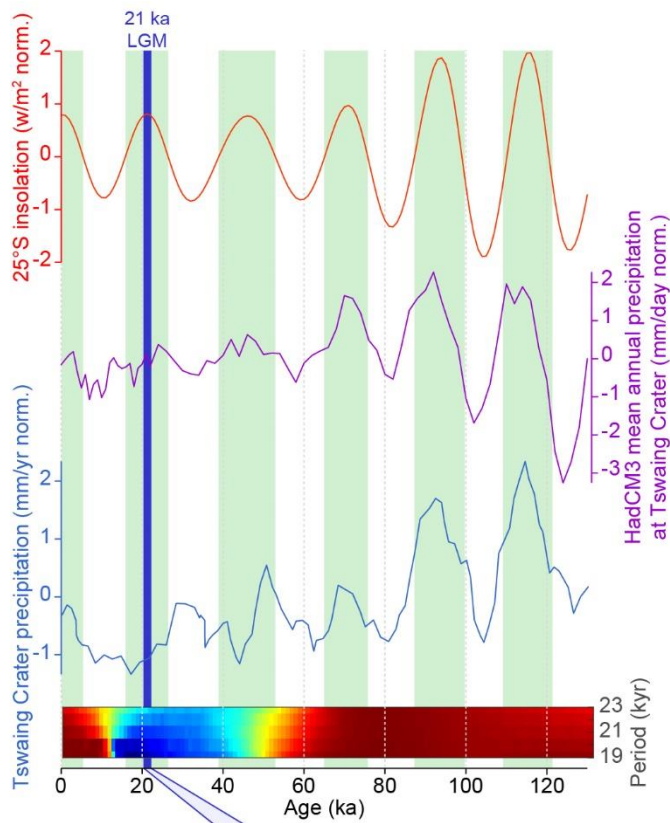


Figure 10: Comparison of austral summer (DJF) insolation at 25°S (Laskar et al., 2004), quasi-transient HadCM3 Earth system model simulation of mean annual precipitation at Tswaing Crater (Gordon et al., 2000; Pope et al., 2000; Singarayer and Valdes, 2010), and the Tswaing Crater precipitation reconstruction (Partridge et al., 1997). Heat map presents results of semblance analysis of HadCM3 and proxy-based precipitation reconstruction for Tswaing Crater (red=positive correlation and blue= negative correlation). Green shading indicates phases of above average summer insolation at Tswaing Crater. The dark blue line indicates the ~21 ka period used by the PMIP3 models, of which the ensemble 21 ka – pre-industrial precipitation simulation is shown in the lower pane (from Chevalier et al., 2017). The location of Tswaing Crater is indicated by the orange dot. Inter-model agreement on the sign of the anomalies at ~75/90%, which correspond to an agreement of seven and eight out of the nine models, is indicated by red dots/crosses, respectively.

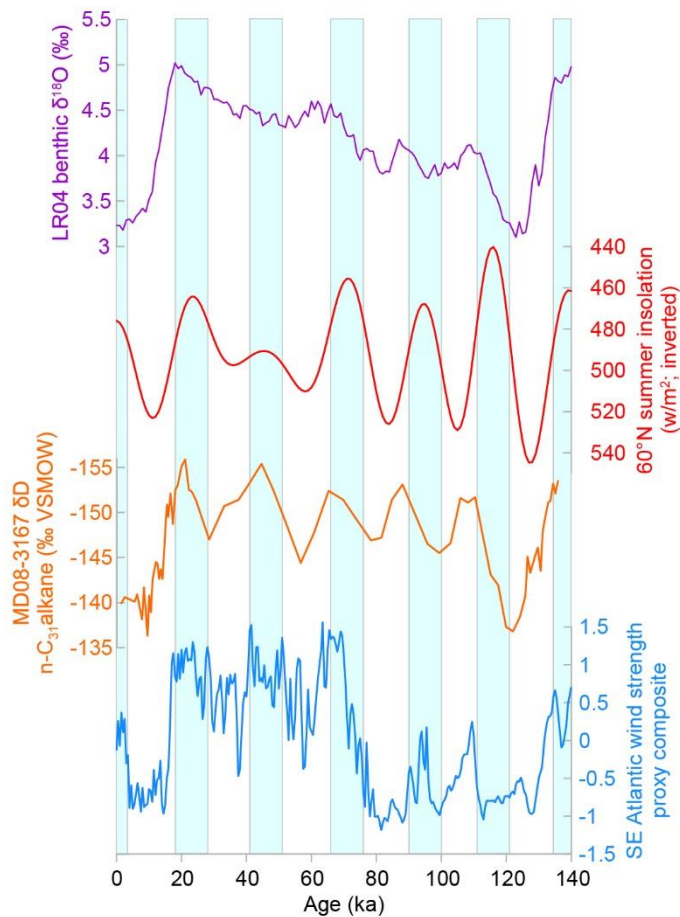


Figure 11: Comparison of LR04 benthic $\delta^{18}\text{O}$ stack (higher values indicate increased global ice volume; Lisiecki and Raymo, 2005), boreal summer (DJF) insolation at 60°N (Laskar et al., 2004), the leaf wax δD record from marine core MD08-3167 (lower values indicate more humid conditions; Collins et al., 2014), and the composite record of SE Atlantic wind strength proxies (higher values indicate increased wind strength; Chase et al., 2019a; data from Farmer et al., 2005; Little et al., 1997; Pichevin et al., 2005; Stuut et al., 2002). Blue bars highlight periods of low boreal summer insolation at precessional wavelengths.